Geophysical Exploration and Dynamics of the Alpine Fault Zone

Tim Stern[1], David Okaya[2], Stefan Kleffmann[1,3], Martin Scherwath[1,4], Stuart Henrys[5], and Fred Davey[5]

The Alpine Fault of central South Island New Zealand, can be tracked with seismic reflection methods to depths of ~35 km as a listric-shaped surface with strong reflectivity. Maximum dips of the surface are ~60 degrees at 15 km depth and the dip then lessens with depth until the reflectivity is sub-horizontal at ~35 km. Wide-angle seismic methods are used to show that the P-wave velocities of the rocks are up to 10% less than normal in the zone above the fault surface. In cross-section this low-velocity Alpine Fault Zone is elongate, sits above the fault surface, and has dimensions roughly 45 by 20 km. A magnetotelluric study shows a low-resistivity anomaly that is roughly coincident with the zone of low seismic velocity. A straightforward interpretation is that both the electrical and seismic anomalies are caused by interconnected fluids at lithostatic pressure. The inference of fluids in the lower crust is supported by an attribute analysis of seismic reflections on specific shot gathers where the Alpine Fault reflections can unequivocally be identified. We reference both the amplitude and phase of the fault-zone reflections to the distinctive side-swipe reflections generated at the far shore of Lake Pukaki. High reflection coefficients of ~0.25 are estimated for the Alpine Fault reflections, which may require both anisotropy and fluid to explain. We interpret the source of water to be metamorphic dewatering of the schist-greywacke rocks that thicken into the orogen. A detachment surface along which the greywacke-schist rocks are obducted is recognised as a zone of strong reflectivity on an 80-km-long, unmigrated seismic reflection section. This zone of strong reflectivity, which apparently merges into the Alpine Fault reflections, does not correlate with depth to the Moho but rather with the boundary between the base of the schist-greywacke rocks (Vp ~6–6.2 km/s) and the lower crust (Vp ~7–7.2 km/s). We interpret the strong reflectivity on this boundary as being due to a shear fabric. Both geological and geophysical observations imply deformation in the lower and mid-crust and mantle that appears to be caused by a combination of ductile and brittle behaviour, with no evidence of lithospheric flexure. We interpret the Alpine Fault Zone as a profoundly hot, wet, and weak region of continental crust.

[1]School of Earth Sciences, Victoria University of Wellington, Wellington, New Zealand.

[2]Dept of Earth Sciences, University of Southern California, Los Angeles, California.

[3]Now at NZ Oil and Gas, Wellington, New Zealand.

[4]Now at GEOMAR, Kiel, Germany.

[5]Institute of Geological and Nuclear Sciences, Lower Hutt, New Zealand.

A Continental Plate Boundary: Tectonics at South Island, New Zealand
Geophysical Monograph Series 175

10.1029/175GM11

1. INTRODUCTION

Our knowledge of the internal structure of continental fault zones is largely based on indirect means including studies of exhumed paleo-faults, seismicity and laboratory studies [*Sibson*, 1986]. More recently, multinational teams are directly sampling fault zones to depths of a few kilometres with advanced drilling methods [*Hickman et al.*, 2004]. Directly imaging faults zones to depths > 1–2 km with seismic methods has, however, proved to be difficult, especially for faults that are near vertical [*Hole*, 1996; *Hole et al.*, 2001]. In this study a successful imaging of New Zealand's Alpine Fault to depths of 35 km is presented. This work formed part of South Island Geophysical Transect (SIGHT) project that was a joint US-New Zealand initiative to image a major continental transform fault to lower crust-upper mantle depths [*Davey*, 1997]. A major focus of the SIGHT experimental design was to take advantage of the narrowness of central South Island, and the dip of the fault, to develop seismic methods that could illuminate the structure of the fault from surface outcrop to lower crustal depths.

The term "Alpine Fault Zone" is here defined as the subsurface downward projection of the Alpine Fault and the triangular area of crustal rocks that constitute the hanging wall of the Alpine Fault. Linked to the main goal of imaging the fault geometry at depth was an additional aim of learning about the mechanical properties of rocks within the broader Alpine Fault Zone. In particular, we set out to use modern geological and geophysical methods so we could detect the presence or otherwise of fluids within the zone. Since the SIGHT project, further questions concerning continental transforms and crustal fluids have been highlighted that may also be addressed by exploration of the Alpine Fault. For example, the structure and strength of the San Andreas Fault of California has been the focus of recent controversy [*Scholz*, 2000; *Zoback*, 2000]. Low heat-flow and principal stress directions being perpendicular to the fault have been argued as evidence that the San Andreas Fault is "weak" [*Townend and Zoback*, 2001]. What the Alpine Fault offers, compared to other continental transform faults, is a fault that penetrates to greater crustal depths as an inclined to listric-shaped zone of shearing and deformation. Such inclined structures are easier to image with seismic methods than vertically orientated faults [*Hole et al.*, 2001].

Mid- to lower-crustal rocks immediately east of the surface trace of the Alpine Fault are being rapidly exhumed via an Alpine Fault "ramp" system [*Wellman*, 1979; *Little*, 2004]. This geometry facilitates the application of seismic methods to extrapolate structures from deep in the crust to the surface of the earth. Furthermore, because of the component of convergence at the Alpine Fault, the fault zone is effectively being loaded by mountain building at the surface of the earth, and also loaded by thickened, and therefore cold, mantle lithosphere pulling from below. This allows us to make another more direct, and general, measure of strength via flexural rigidity of the lithosphere.

In this paper we present a summary of geophysical data that pertains to the structure of the Alpine Fault Zone at depth. We quantitatively estimate its strength from flexural rigidity due to loading. We also make an assessment of fluid pressures, from seismic and electrical observations, within the Alpine Fault Zone. We also discuss our results in light of recent research on strain release by low–frequency earthquakes in other regions that are dominated by high fluid pressures. Finally, we comment on the potential of the Alpine Fault Zone to be a source of exploitable energy.

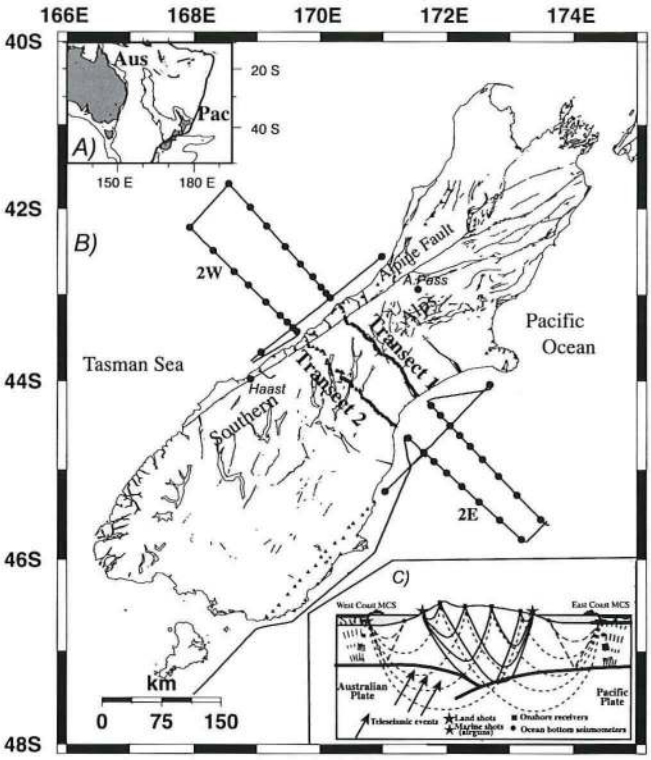

Figure 1. a. Plate setting for the South Pacific and Australian (Aus) and Pacific (Pac) plates. b. Location map for Transect 1 and 2 (referred to as T1 and T2 in text). Off-shore lines are tracks for the multichannel seismic lines and solid dots represent locations of ocean-bottom seismographs. On both transects 1 and 2 about 400 portable seismographs were deployed. Twenty-one land shots with 300–1000 kg of explosives per shot were detonated in 50 m deep bore holes. Including cross lines, about 1000 seismograph deployments were made for the whole project. c. A cartoon depicting the geometry of ray paths for onshore–offshore shooting, onshore shots, and teleseismic arrivals.

2. CRUSTAL STRUCTURE FROM THE SIGHT PROGRAMME

Programs of passive seismology, magnetotelluric and electrical studies, petrophysics as well as crustal-scale reflection profiling, and refraction-wide-angle reflection profiling were associated with the SIGHT study [*Davey*, 1997; *Stern et al.*, 2000; *Okaya et al.*, 2002]. Buried shots of ~1000 kg of explosives were used on land for refraction shooting, whereas the reflection-wide angle work was anchored by marine multichannel seismic (MCS) profiling; both onshore seismographs and ocean-bottom seismometers (OBS) recorded the MCS airgun sources. These data were collected in 1996 along two parallel transects across central South Island (Figure 1).

What made the SIGHT programme both unique and effective was its two-sided onshore–offshore component that allowed efficient coast-to-coast imaging. Onshore–offshore seismic methods across "continental islands", of dimensions similar to that of central South Island, allows high resolution of crust and upper mantle structure [*Okaya et al.*, 2002]. With island widths of 100-250 km, powerful ship-mounted air-gun arrays, deployed each side of the island, provide optimal coast to coast coverage of structure beneath the island (Figures 1 and 2). Combining the onshore-offshore experiment on each side of the island with

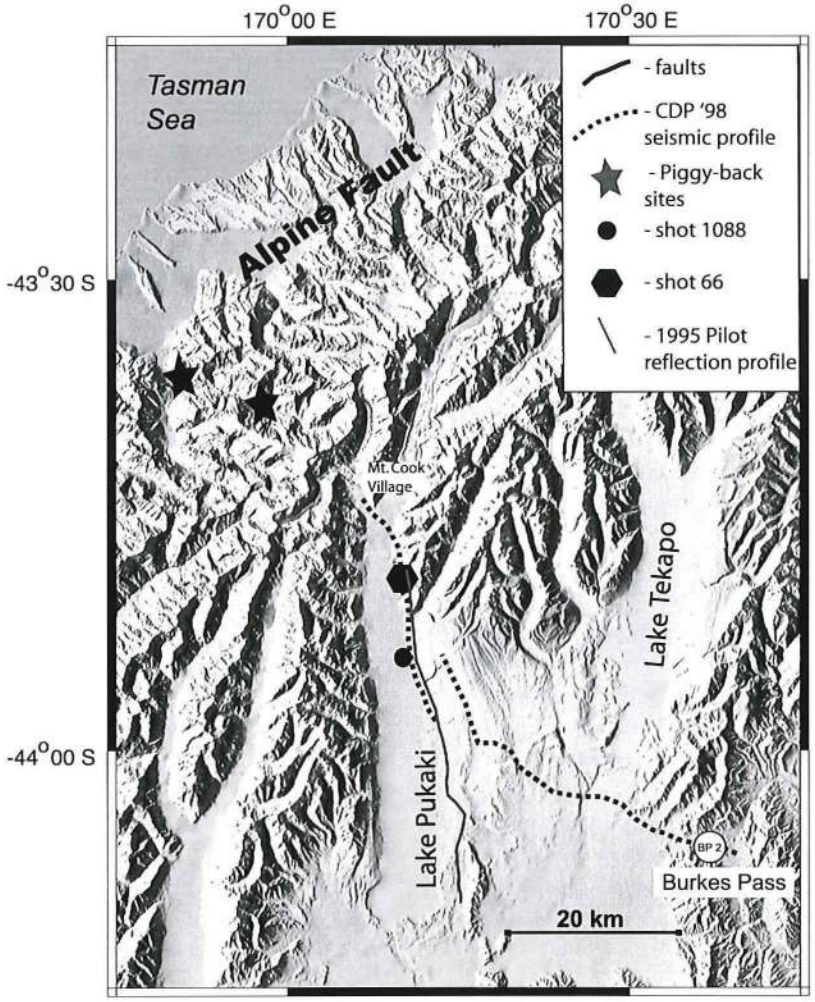

Figure 2. Location of other seismic reflection profiles associated with transect T2. Thin black line shows position of the Pukaki'95 experiment described in *Kleffmann et al.* [1998]. Black dashed-line shows position of the CDP'98 profile described in the text, which is in two portions separated by a large topographic scarp. The position of "piggy-back" sites on the west coast used to record wide-angle reflections shots from CPD'98 are shown [*Stern et al.*, 2001]. Positions of shot 1088 (Pukaki'95) and shot 66 (CDP'98) are shown. White circle at Burkes Pass is position of shot BP2 discussed in text.

the land refraction profiles permitted shot "super gathers" of approximately 600 km in length to be created [*Okaya et al.*, 2002].

Teleseismic events from the western Pacific were serendipitously recorded across the onshore seismograph arrays during the 7-day window of seismic profiling. These data provide important constraints on structure of the mantle beneath South Island [*Stern et al.*, 2000]. Because the teleseismic waves from the western Pacific come up through the crust at a steep angle, they also illuminated structure within the Alpine Fault Zone (Figure 1c).

Most of the data collected by SIGHT possess high signal to noise ratio with strong Pn phases recorded to offsets of ~300 km [*Scherwath et al.*, 2003]. Strong PmP, SmS, and PmS phases from both air guns and land shots were recorded from the airgun shots [*Pulford et al.*, 2003].

Crustal Structure Images

A combination of forward modelling and tomographic inversion was used to create crustal-upper mantle structure images of the plate boundary [*Scherwath et al.*, 2003; *van Avendonk et al.*, 2004]. Principal features and interpretations to note are (Plate 1a and b):

1. A crust that increases in thickness from 27 km at the coasts of South Island to a maximum of 44 km just east of the main divide of the Southern Alps on transect 2. This increase (~17 km) in crustal thickness is nearly twice that required to isostatically support the average topography of South Island.
2. Seismic P-wave speeds of 6–6.3 km/s throughout most of the crust except for two regions of lower wave speed directly beneath the Southern Alps on both transects. These zones of low Vp are interpreted as being due to enhanced fluid pressure associated with the release of metamorphic fluids into the lower crust [*Stern et al.*, 2001; *Wannamaker et al.*, 2002].
3. Seismic wave speeds of ~8.1 km/s in the mantle, except for a zone that extends 100 km on each side of the Alpine Fault in which strong anisotropy in Pn is detected [*Scherwath et al.*, 2003; *van Avendonk et al.*, 2004]; see later section.

These observations underpin the following compilation and analysis of data related to the Alpine Fault that includes: analyses of the geometry and phase and amplitude of fault zone reflections; delay times of wide angle reflections that pass through the Alpine Fault Zone; and an analysis of both unmigrated and migrated seismic reflection section from the eastern side of the Alps.

3. FAULT ZONE REFLECTIONS

In March 1995, a pilot seismic reflection and piggyback wide-angle seismic reflection experiment was carried out along the eastern shore of Lake Pukaki (Figure 2). Advantage was taken of a straight and isolated road along the NE shore of the lake. Here a 6 km long, 120 channel, spread was laid out along the road and shots of 25 kg were detonated at a water depth of 20 m in the adjacent lake. Shots were offset by 4 km to the south of the 120-channel spread [*Kleffmann et al.*, 1998]. At the northern end of the lake, the seismic line is about 45 km from the Alpine Fault and at an azimuth of about 60° to the strike of the fault (Figure 2).

A shot gather from the northern end of the line shows good signal to noise ratio where the seismic array was north of the edge of the lake and extended into an area floored by river gravels rather than glacial till (Figure 3a). A series of deeper crustal reflections can be seen in the last 60 channels of the shot gathers where the geophones were in near-surface river gravel. At 9 s two-way-travel-time (twtt) there is a prominent reflection with "reverse moveout"; i.e., the reflection occurs at progressively earlier times on geophones with increasing offset from the shot. Such reverse-moveout is typical of reflections that have come from a dipping reflector where the dip is towards the geophone spread (Figure 4a and b). After filtering in the F-K domain the reverse moveout reflections are clearer (Figure 3b). In particular, a further stronger event is now evident at about 13 s. Together with the 9 s reflection these define a zone that is ~4 s twtt thick. If a mean P-wave speed of ~5.5–6 km/s is assumed for the zone, its thickness is on the order of 11–12 km.

Position and Dip of Alpine Fault Reflectors

The arrival time for a reflection from a planar reflector with dip ϕ is described by a hyperbolic equation given by:

$$T^2 = 4\,Z^2/V^2_{rms} + X^2/V^2_{rms} + 4\,(Z/V^2_{rms})\,X \sin\,\phi \qquad (1)$$

where T is the travel time, Z is the depth to the reflector and V_{rms} is the "root mean square" velocity between the reflector and the ground surface [*Sheriff and Geldart*, 1995] and X is geophone offset either positive or negative for shooting down-dip and up-dip, respectively.

If Equation 1 is plotted for values of X between 4 and 10 km and V_{rms} = 5900 m/s, it can be seen that the magnitude of negative moveout across a spread is a sensitive measure of dip of the reflector (Figure 4a). We measure the nega-

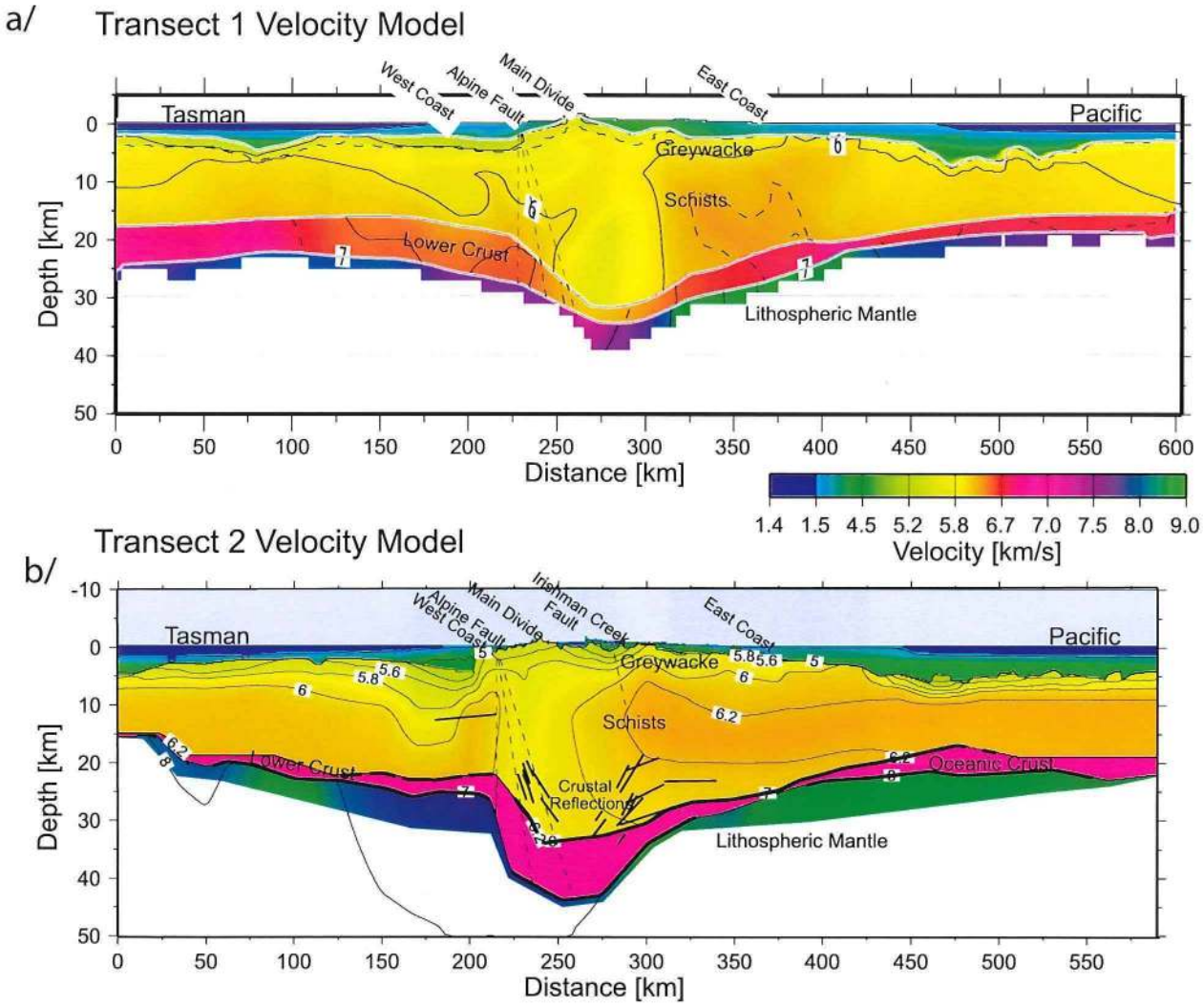

Plate 1. a. Crustal structure image of transect 1 [after *Okaya et al.*, 2002; *van Avendonk et al.*, 2004]. 5× vertical exaggeration. Note low-velocity zone in crust beneath Southern Alps. Dashed lines emanating from surface trace of Alpine fault represent theoretical dips of 0, 60 and 45 degrees. b. Crustal structure cross-section for transect T2 at 5× vertical exaggeration [*Scherwath et al.*, 2003]. Black bars show positions of strong seismic reflectors discussed later. Note region of low seismic velocity in crust beneath Southern Alps and low upper mantle seismic velocities beneath and west of Alpine Fault.

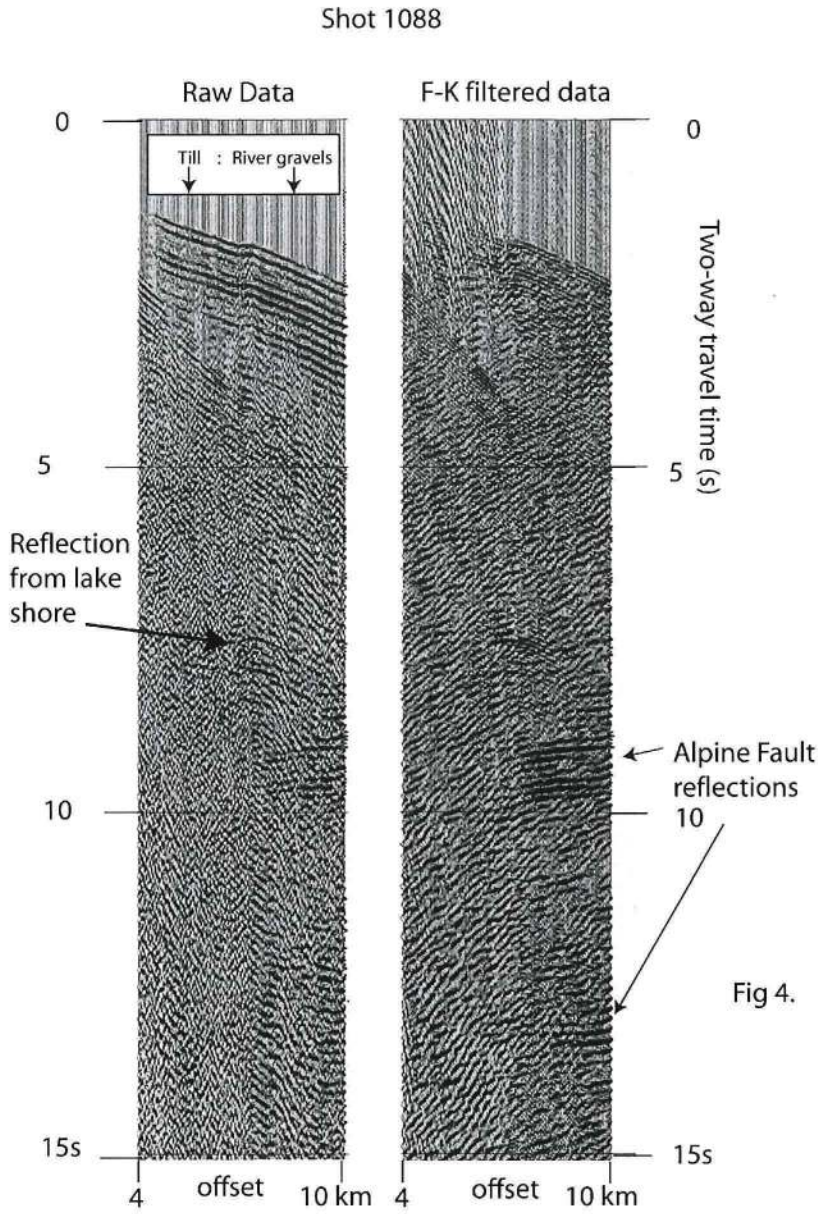

Figure 3. Shot gather shot 1088. Location shown in Figure 2. Spacing between phones is 50 m, which gives a 5950 m spread length for 120 channels. Offset to shot is 4 km and in the lake to south of the spread. Panel on left shows data passed through 20 s AGC and broad band-pass filter. Note how data improve for far offsets as the geophone spread spanned a transition from glacial tills (first 60 channels) to sorted river gravels (last 60 channels). Curved event ~7 s twtt is interpreted to be a side-swipe reflection from the far side of lake. Deeper reverse moveout reflection events at 9–13 s twtt are interpreted to be from the dipping Alpine Fault zone. Panel on left shows same data filtered with an F-K filter that suppresses all events that dip to the right. This filter enhances the 9 s event and brings out an event at 13 s that would not otherwise have been seen.

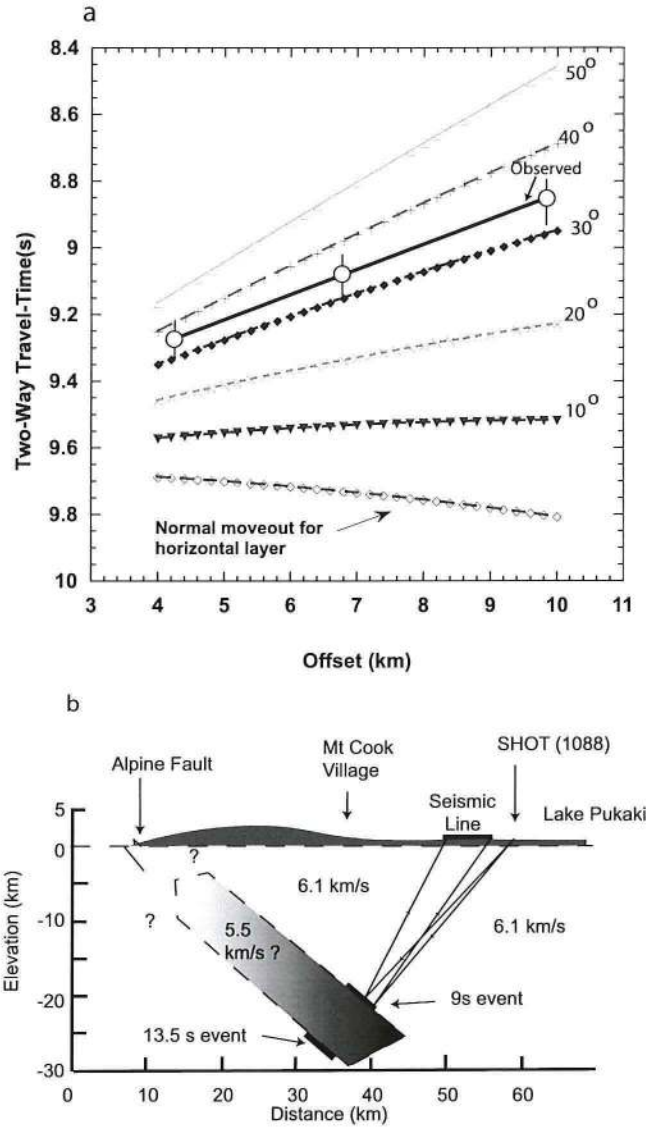

Figure 4. a. A plot showing theoretical moveout for a reflector that is 30 km deep in a constant velocity 6 km/s medium. Different curves are shown for dips between 10 and 50 degrees in the offset range of 4 to 10 km, appropriate for shot 1088. Also shown is the observed moveout for the 9 s event on shot 1088 including estimated uncertainties. Interpreted apparent dip of ~34 ± 5°. It is an apparent dip because the shooting line is at an angle to the dip-plane of the fault plane (see text). b. Schematic interpretation of reflectors from shot gather 1088 based on just ~4 km of shot gather data. Note that the projection of the reflectors to the surface approximately corresponds with surface trace of Alpine Fault. Spacing between geophones = 50 m.

tive moveout, across the 6 km long spread, on a number of adjacent shot gathers to be 380 ± 20 ms and plot it against the calculated negative moveouts for dips ranging between 10 and 50 degrees (Figure 4a). The best fit for the reflector dip from measuring individual segments on shot gathers range between 33–40° [*Davey et al.*, 1995; *Kleffmann et al.*, 1998]. For shot 1088 we estimate the dip as 35 ± 5° at a depth of ~25 km beneath Mt. Cook Village (Figure 4b). If the reflection is from the downward projection of the Alpine Fault then the dip estimate is only an apparent dip given that the azimuth of the seismic array was aligned at 60° to the Alpine Fault (Figure 1). For a shooting line that is not in the direction of dip, the angle δ is the apparent dip, which is related to the true dip ϕ by *Dobrin* [1976]:

$$\sin \delta = \cos \theta \sin \phi \qquad (2)$$

where θ is the angle between the shooting line and the direction in which the reflector dips. Thus for $\delta = 35°$ and $\theta = 30°$ the true dip of the reflector is $\phi \approx 40°$. A simple interpretation is that the reflector is a perpendicular distance of about 30 km from the shot, and thus at a depth of about 25 km directly below Mt. Cook (Figure 4b). When projected upward the dipping reflector intersects the surface close to the surface trace of the Alpine Fault.

It is not clear if the reflection is due to an acoustic impedance contrast between two different rock types each side of the fault, or if it is due to physical property changes within the fault zone itself. Field observations from the Alpine Fault outcrop [*Grapes and Watanabe*, 1992; *Norris and Cooper*, 2003; *Little*, 2004] shows a 1–2 km wide zone of strongly foliated mylonite dipping at ~45 degrees, which is overlain by ~15 km thick section of high grade schist. The mylonites are one possible source for the strong reflections given their strong foliation. They are, however, only observed to be 1–2 km thick in surface outcrop [*Norris and Cooper*, 2003] and the zone of reflectivity we see is more than 10 km thick. In order to resolve these differences we need to try to quantify the acoustic impedance contrast of the reflector.

4. ATTRIBUTE ANALYSIS OF ALPINE FAULT REFLECTION

An 80-km-long crustal scale seismic reflection profile (CDP'98) was collected in 1998 as part of SIGHT in an attempt to track the Alpine Fault to depth (Figure 2). CDP'98 was carried out in the Southern Alps foothills within the Pacific plate using 50 kg explosive sources and a commercial 850 channel seismic recording system. At a nominal 40 m

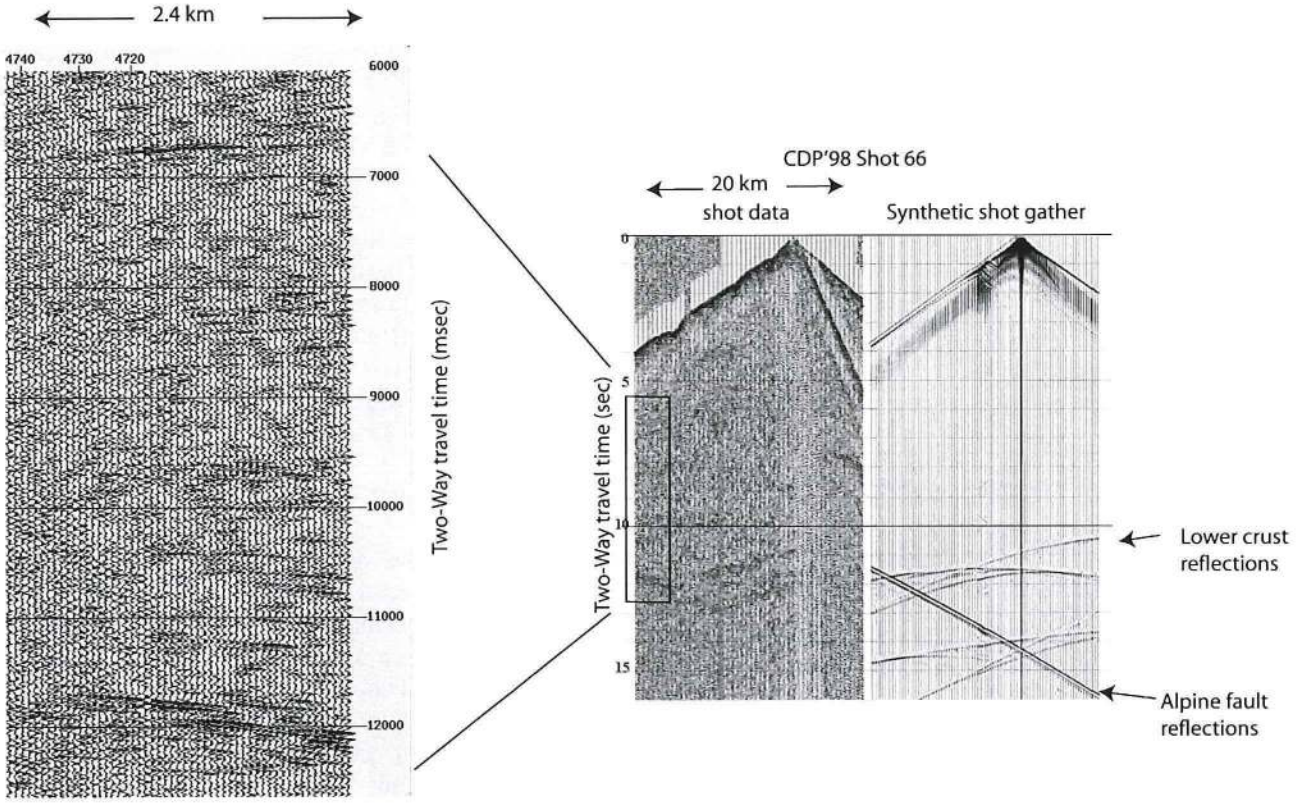

Figure 5. Data from shot 66 of the CDP'98 project. Spacing between geophones = 40 m. Location shown on Figure 2. Blow up on left shows the 2.4 km long part of the shot gather where both reflections from lake shore (6500 msec twt) and Alpine Fault (1200 msec twt) occur on common traces. Synthetic on right shows the predicted position for a reflection from a 60° southeast-dipping reflector that outcrops at the surface trace of the Alpine Fault [*Okaya et al.,* 2007].

spacing for geophones, the length of the seismic array here was ~34 km, compared to 6 km for the Pukaki'95 experiment (Figure 3). Shot-gathers from this experiment also showed the reverse-moveout Alpine Fault reflections but over a larger offset range (Figure 5).

From both the 1995 and 1998 experiments a strongly curved event between 6 and 7 s twtt is observed (Figures 3 and 5). This event had such large moveout (high curvature) that it initially proved puzzling. Its normal moveout (NMO) velocity is about 1.7 ± 0.3 km/s, which is close to the speed of seismic P-waves in water [*Kleffmann et al.*, 1998]. Furthermore, the timing of 7 s twtt, combined with the NMO velocity, makes it impossible for it to be a reflection from a horizon within the solid earth. Our interpretation of this large moveout event is that it represents a horizontally travelling ray through Lake Pukaki that has reflected off the far western side of the lake and come back to the geophone spread. The distance across the lake is about 5 km and the western and eastern lake-shores are remarkably parallel (Figure 2). The travel time from shot to reflection point and back to geophone is approx. 2 × distance /velocity = (2 × 5 km)/1.5 km/s ≈ 6.7 s, which is in the range of the observed reflection. This "side-swipe" event is particularly useful as we can readily calculate the acoustic impedance contrast between lake water and rock, thereby providing a standard of comparison for the amplitude and phase of deeper events (Plate 2).

Where both lake-shore and Alpine Fault events occur on the same trace we perform attribute analyses on their relative phase and amplitude (Plate 2). The phase of an event in a seismogram represents the polarity of the particle motion of the seismic wave, which can be positive or negative. A reflection will have a positive or a negative phase depending on whether the acoustic impedance at the reflector is positive or negative for a down-going wave. For near vertical incidence waves, the acoustic impedance contrast at a horizontal interface between an upper layer 1 and a lower layer 2 is defined by:

$$\Delta Z = (Z_2 - Z_1)/(Z_1 + Z_2) \qquad (3)$$

where $Z_1 = V_{P1}\rho_1$ is the acoustic impedance of layer 1, where V_p and ρ are the P-wave velocity and density. ΔZ is a quan-

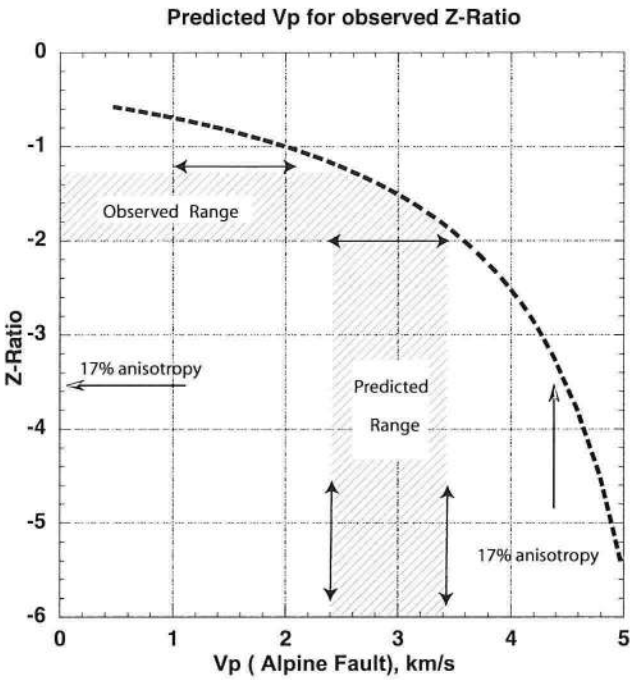

Figure 6. Iterative solution to Equation 4 showing the relationship between the range of observed ΔZ ratio and the required value range of P-wave velocity in the Alpine Fault Zone (Equation 4). Adopted parameters for velocity and density shown in Table 1. Also shown is the predicted, maximum, drop in P-wave velocity for 17% anisotropy (i.e., 5.5 to 4.5 km/s) and the consequent ΔZ ratio. Note that this ratio is still roughly 2 times what is observed. In order to get down to observed ΔZ ratio, V_p in the Alpine Fault Zone has to be lowered by ~50% or other processes need to be proposed (see text).

tity that expresses the ratio of the reflected and transmitted amplitudes often called R, the reflection coefficient [*Sheriff and Geldart*, 1995].

The phase of the first coherent lake-shore reflection appears to be positive on the attribute plot (pink in Plate 2a), which is consistent with the contrast between low P-wave speed in water and the high P-wave speed in rock. In comparison, the first distinctive pulse from the Alpine Fault has opposite polarity (blue in Plate 2a). We therefore interpret the Alpine Fault zone reflector as having a negative impedance contrast. This dual visual comparison was performed on several gathers and on many traces. In general, the analysis gave a reverse polarity for the Alpine Fault reflector, but not always. In about 15% of the cases the same polarity was evident. Because some events have normal polarity we conclude that the reflections arise from a fault zone that consists of alternating negative and positive impedance contrasts but the zone is laterally variable.

We make an estimate of A_{lake}/A_{Afault} (ratio of amplitude as measured in arbitrary units on a common trace) from an amplitude comparison between the lakeshore reflection and the Alpine Fault reflection (Plate 2b and 7c). Shot gathers were analysed with little processing apart from a broad band-pass filter and an Automatic Gain Control (AGC) window of 20 s. This serves to even out the gain over 20 s but will have negligible effect on the true relative amplitudes between the reflections of interest at 7 and 11 s twtt.

We make the approximation [*Sheriff and Geldart*, 1995]:

$$A_{lake}/A_{Afault} = \Delta Z_{lake}/\Delta Z_{Afault} \quad (4)$$

The assumption here is that there is only a small change in the incident wave amplitude between 7 and 11 s twtt due to spherical divergence [*Sheriff and Geldart*, 1995].

As for the phase analysis we observe a variety of amplitude responses with the two extreme ones shown in the example of Plate 2b and c. This range of A_{lake}/A_{Afault} is 1.3 to 2.0. Thus for ΔZ_{lake} ~0.5 (Table 1) we estimate ΔZ_{AF} to be between 0.25 and 0.33. For a lower crustal reflection this is high compared to other estimates of reflectivity from the lower crust. Most maximum observed values of the reflection coefficient for reflectors in the lower crust are around 0.2 [*Warner*, 2004]. Assuming near vertical incidence, the ratio of impedance contrasts (Z ratio) is:

$$\Delta Z_{lake}/\Delta Z_{Afault} = [(Z_{tg}-Z_w)/(Z_{tg}+Z_W)] * [(Z_{af}-Z_g)/(Z_{af}+Z_g)]^{-1} \approx 1.5\text{–}2.0 \quad (5)$$

Here subscripts tg, w, af, and g on the acoustic impedance (Z) refer to till-gravel, water, Alpine Fault and greywacke respectively. Values of Z for all quantities except Z_{af} are known (see Table 1) and thus Z_{af} can be solved for by iteration.

Petrophysical work shows a negligible variation in density, ρ, for schist-greywacke rocks from within the Alpine Fault Zone [*Garrick and Hatherton*, 1973]. Accordingly, as $Z_{af} = V_{af}\rho_{af}$ a range of V_p between 2.5 and 3.5 km/s is predicted for the Alpine Fault Zone (Figure 6). This is a drop of between 30 and 60% of its host rock (greywacke-schist) values (Table1). Observed P-wave seismic velocities within the Alpine Fault Zone, as measured along ray paths tens of km in length, have dropped by only 10% compared to the host rock [*Stern et al.*, 2001], so we seek additional explanations for the strong reflectivity within the Alpine Fault Zone. Two possibilities are anisotropy and fluids.

Maximum measured anisotropy of a suite of high grade Haast Schists and mylonites is 17% [*Okaya et al.*, 1995]. A 17% anisotropy would produce a Z-ratio (Equation 5) of ~3.5 (Figure 6), which is greater than what is observed.

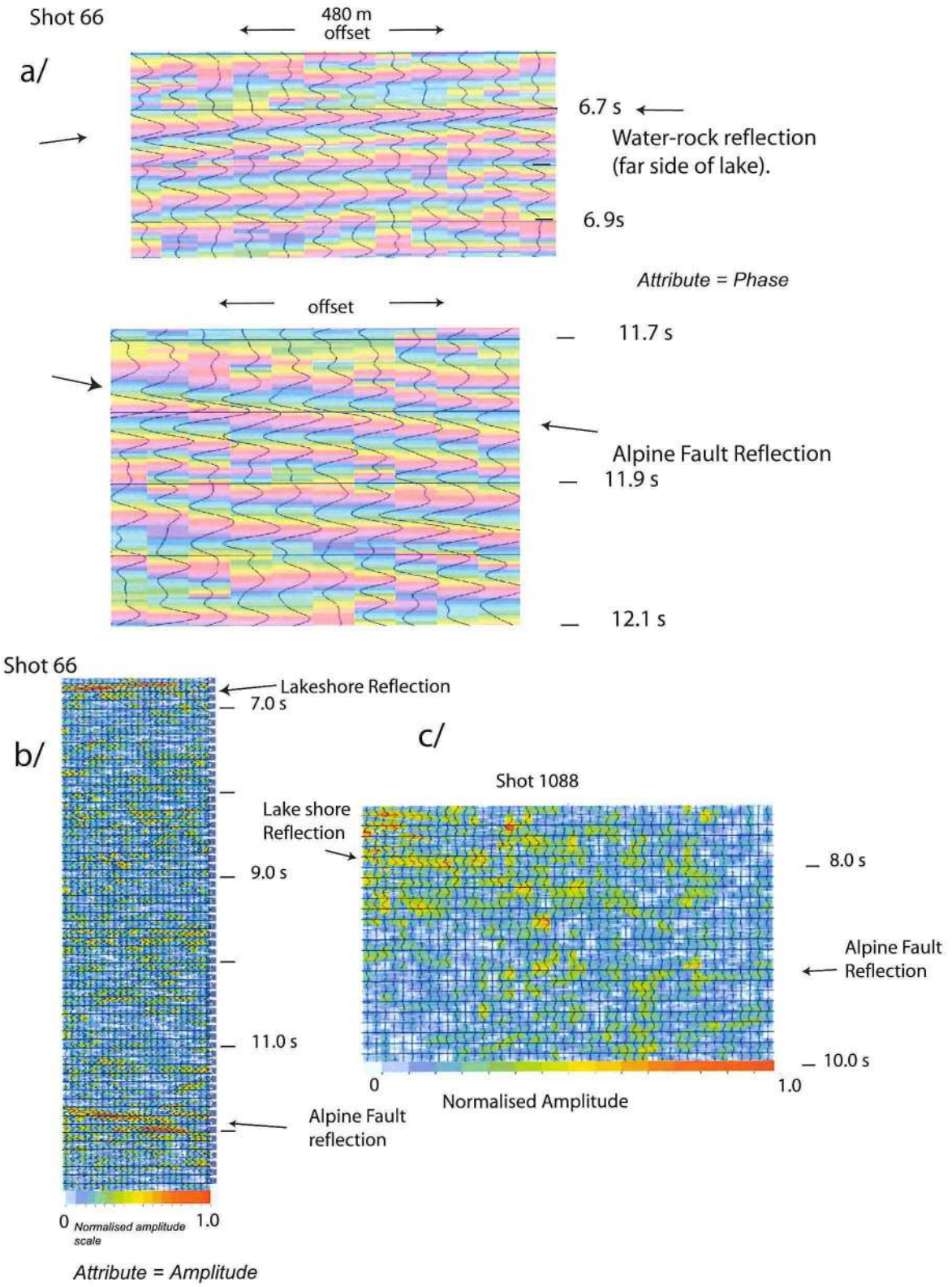
Shot 66
480 m
offset
a/
6.7 s
Water-rock reflection
(far side of lake).
6.9s
Attribute = Phase
offset
11.7 s
Alpine Fault Reflection
11.9 s
12.1 s
Shot 66
Lakeshore Reflection
7.0 s
b/
c/
Shot 1088
Lake shore
Reflection
9.0 s
8.0 s
Alpine Fault
Reflection
11.0 s
10.0 s
0
1.0
Normalised Amplitude
Alpine Fault
reflection
0
Normalised amplitude
scale
1.0
Attribute = Amplitude

Table 1. Data used as input to impedance contrast analysis. [After *Kleffmann et al.*, 1998; *Kleffmann*, 1999].

Rock Type	P-wave Velocity km/s	Density Mg/m^3	Acoustic impedance Z = velocity*density (Mg m^{-2} s^{-1})
Greywacke-Schist	4.5–6	2.7	13.5
Shallow Glacial till	1.8–2.3	2.3	4.6
Water	1.5–1.55	1.0	1.5
Alpine Fault Zone rocks	?	2.7	?

Other means of enhancing the reflectivity could be constructive interference within layers of contrasting schist grade, or pockets of fluid saturated rock within the Alpine Fault Zone [*Warner*, 1990]. The source rock for this strong reflectivity is discussed further after other seismic indicators of structure are considered.

5. DETECTION OF LOW SEISMIC WAVE SPEEDS WITHIN THE ALPINE FAULT ZONE

Evidence for a low-speed region in the hanging wall of the Alpine Fault initially came from a 1983 reconnaissance seismic refraction survey of the central Southern Alps [*Smith et al.*, 1995]. This analysis was based on three large shots recorded by 17 analogue seismographs distributed along Transect 2 (T2) (Figure 1). The identification of the low-speed region was based on anomalous delays at just one seismograph. Later work, however, within the main SIGHT project collected seismic refraction data on 400 seismographs along T2 from shot 27 west of the Alpine Fault (Figure 7). These data show that, with respect to a well–determined velocity model for the upper-crust [*Kleffmann et al.*, 1998], delays for Pg occur for rays that turn through the top of Alpine Fault Zone [*Kleffmann*, 1999]. The delays increase with offset out to 70 km beyond which they are constant at ~0.3–0.4 s (Figure 7a).

Based on forward modelling, the zone where these delays start to occur can be isolated to the shaded box in Figure 7a [*Kleffmann*, 1999]. The length of the shaded region is ~16 km. For a time delay Δt, along a path Δx where the velocity has been reduced from V_1 to V_2, we have:

$$\Delta t = \Delta x(1/V_1 - 1/V_2) \quad (6)$$

If we let V_1 be 6.2 km/s, the value of V_2 can be solved to be 5.5 km/s, which is a reduction of 11%.

A larger delay is seen for the lower-crust reflection (P_1P) phase (Figure 7b) [*Kleffmann*, 1999]. From shot 27 there are systematic delays of 0.6–0.8 s for reflections from a lower crust reflector recorded on seismographs to the east of the Southern Alps. The position of, and velocities above, the lower crustal reflector are well controlled from shots east of the Southern Alps. Hence the delay is confined to a path sector along the inclined path from the shot down to the reflector.

These delays were confirmed by a separate experiment that reversed shot 27 (Figure 7b) and "piggy-backed" off shots from the CDP'98 profile (Figures 2 and 8) [*Stern et al.*, 2001]. Two high-resolution, 48-channel, exploration seismographs were located in the valleys of the west coast and recorded the 50 kg shots from the CDP experiment on eastern South Island (Figure 8). If the regular average, eastern South Island, P-wave speeds of 6–6.2 km/s are used for the crust, then the arrivals at the west coast seismographs are 0.8 ± 0.1 s late (Figure 8b); a similar delay found from shooting in the opposite direction (Figure 7b). The length of the wide-angle ray path from the lower crustal reflector to the surface is about 50 km. Using Equation 6 with Δx = 50 km, Δt = 0.8s, and V_1 = 6.1 km/s gives the predicted velocity in the low-velocity zone to be ~5.6 km/s, similar to that calculated from delays in Pg (Figure 7a).

Plate 2. (opposite) a. Attribute analysis for phase. Colour is linked to whether the seismic trace deflects left or right. On top plot the deflection, or "first break", of the first coherent and energetic reflection from the far side of the lake is shown in red. This reflection is from water to rock, from low to high acoustic impedance, and is thus designated to be a positive impedance contrast. On the lower plot the first impulsive reflection from the Alpine Fault can be seen to deflect in the opposite direction and is shown as blue. This indicates a negative impedance contrast for this part of the Alpine Fault reflector. (Attribute analysis carried out with Claritas™ software). b. Attribute analysis of shot 66 for amplitude. The colour scale is normalised as shown at the bottom in an arbitrary linear scale between 0 and 1. Note that lake-shore and Alpine Fault reflectors occur on common traces. Using this record we estimate that the lake-shore reflection is 1.5 times larger than that of the Alpine Fault reflection (amplitude analysis carried out with Claritas™ software). c. As for 7b but on shot 1088. Where there are common overlapping traces the lake-shore reflection is estimated to be ~2 times greater than the Alpine Fault reflector in amplitude.

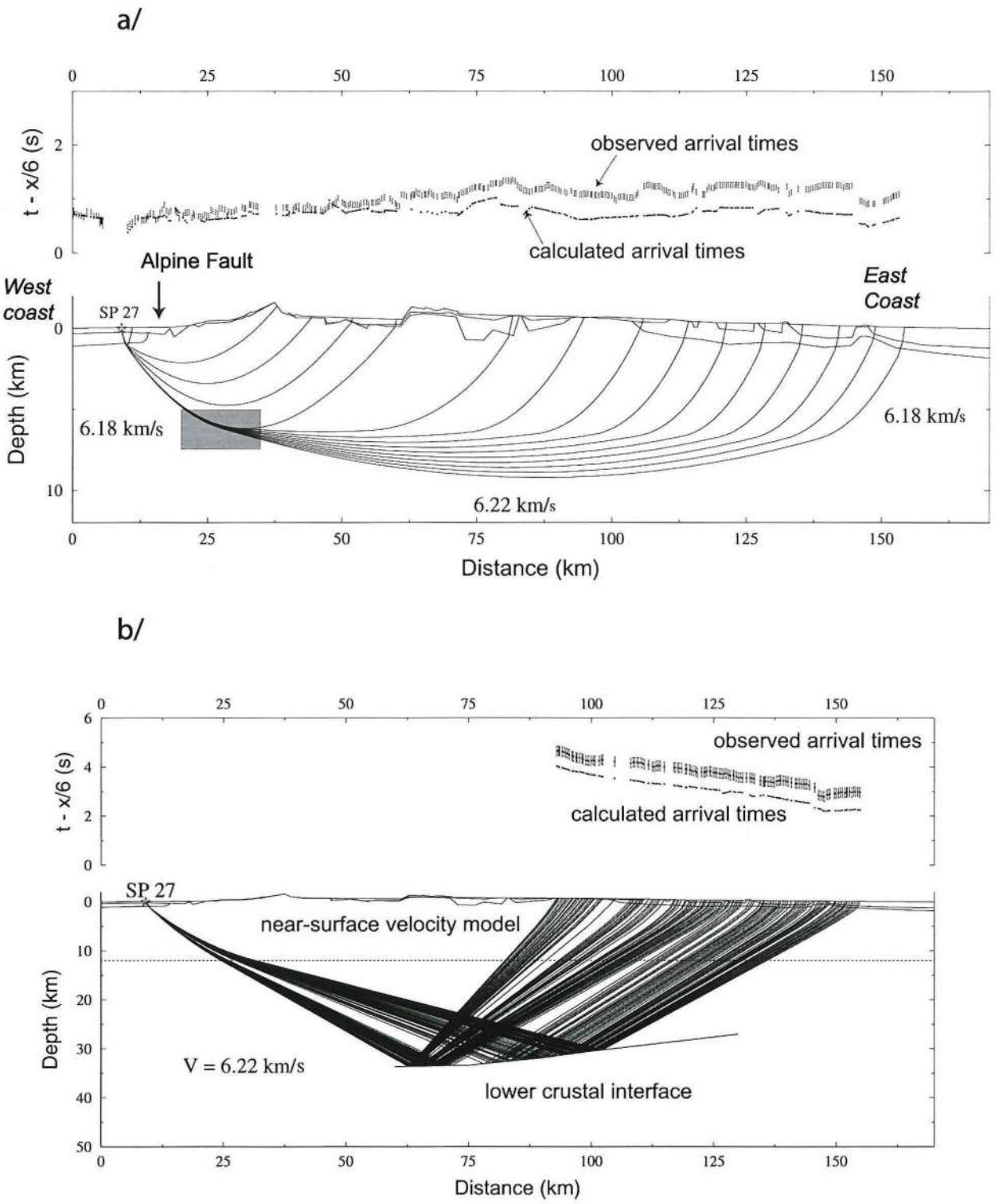

Figure 7. a. A plot of observed and calculated arrivals for shot 27. A simple velocity model [*Kleffmann et al.,* 1998] and then 6.18 km/s below 5 km is used. The shallow velocity structure is based on analysing data from the series of 7 shots along transect T2 [*Kleffmann,* 1999]. Note that a progressive misfit develops out to offset of about 75 km and then stays constant at about 0.35 s. The source zone for the misfit lies in the shaded box shown. A ~11% drop in velocity is required within shaded box (see text). b. Misfits for the arrivals for wide-angle reflections recorded on the eastern side of South Island from shot 27. The wide-angle reflections come from a strong lower crustal interface whose position has been well located by a series of shots east of the Alps. The same shallow velocity structure as in Figure 7a was used but 6.22 km/s was used below 10 km.

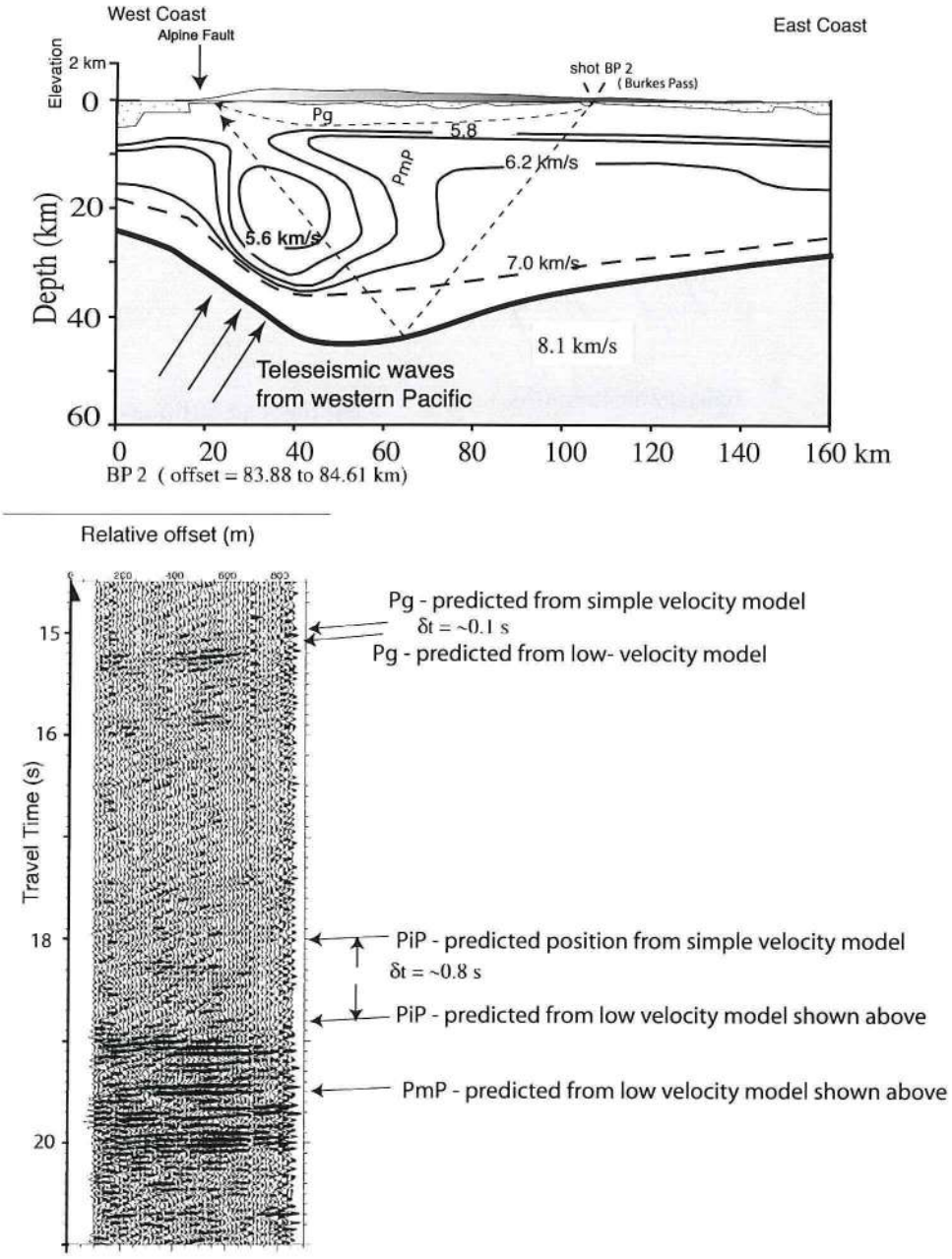

Figure 8. a. A summary model for the low-velocity zone beneath the Southern Alps based on delayed wide-angle reflections and delayed teleseismic P-wave signals. The shot gather shown is from shot BP2 of the CDP'98 project. Location of the shot is shown in Figure 2. Note the wide-angle reflection profile is reversed, i.e., shot 27 from west to east and CDP'98 shots to piggy-back array (Figure 2) from east to west. b. Shot gather from shot BP2 recorded on the piggy-back array (Figure 2) on the west coast, just east of the Alpine Fault [*Stern et al.,* 2001]. The geometry of the shot and receiver is shown in Figure 10a. Geophone spacing is 16 m, and spread length 752 m. Offset from shot is 85 km. The arrows indicate where arrivals are predicted for a simple model (no low-velocity zone) and a model with the low velocity zone shown in Figure 10a. A clear misfit of ~0.8 s is evident.

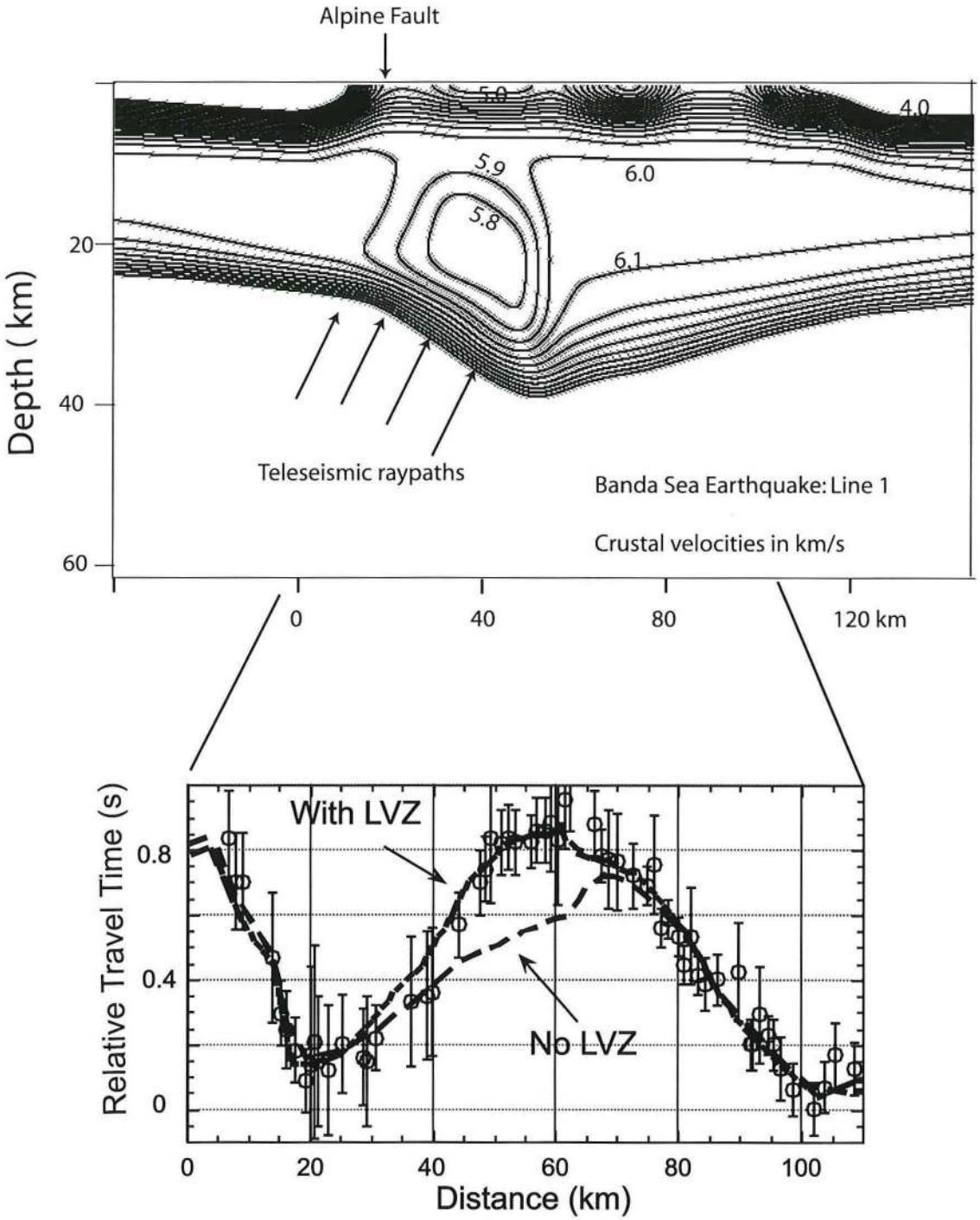

Figure 9. Plot of teleseismic P-wave delays for ray paths that pass through the Alpine Fault Zone. Delays are shown for an earthquake from the Banda Sea recorded on T1. The long-dashed line fit is for a model showing a deep body of thickened mantle as described more fully by *Stern et al.* [2000]. That study noted the shorter wavelength misfit for all models where the ray-paths travelled through the Alpine Fault Zone. Here we show a solution (short-dash lines) that include the low velocity regions shown by closed iso-velocity contours. Similar delays due to a low speed zone are also seen on T2. This set of teleseismic delays are combined with delays of PmP and Pg to produce the crustal low velocity model shown in Figure 8a.

The low-velocity zone is also detected by teleseismic arrivals that pass perpendicularly through the Alpine Fault and Alpine Fault Zone [*Stern et al.*, 2000]. Two earthquakes from the western Pacific recorded on both SIGHT transects give four independent data sets that show delays of ~0.2 s. An example is shown in Figure 9. The forward modelling solution to the low velocity zone is shown in Figure 8a, which incorporates the teleseismic delays of ~0.2 s perpendicular to the LVZ, the Pg delay of ~0.3 s (Figure 7a) and the wide-angle delay of 0.8 s parallel to the low velocity zone is shown in Figure 8b. This low-velocity structure has an apparent maximum thickness of 30 km, a depth extent of 35 km and a slant length of about 45 km.

High fluid pressure is postulated as the source of the low-velocity zone [*Stern et al.*, 2001]. Laboratory data show that for low porosity crustal rocks the compressional velocity will by reduced by10% when the pore pressure approaches lithostatic [*Jones and Nur*, 1984]. A fluid origin for the low-speed zone is further supported by a magnetotelluric study [*Wannamaker et al.*, 2002] along Transect T1 that shows a region of low (~40 ohm-m) resistivity in the crust that is approximately coincident with the low-speed zones [*Henrys et al.*, 2004; *Stern et al.*, 2001]. Interconnected fluid is required to produce the magnetotelluric anomaly, whereas fluid under a pressure approaching lithostatic is necessary to reduce seismic wave speeds by the requisite 10%.

Immediately beneath the trace of the Alpine fault fluid-flow is dominated by local convection of meteoric water with little metamorphic signature [*Vry et al.*, 2001]. In contrast, geological [*Koons et al.*, 1998] and geophysical studies [*Wannamaker et al.*, 2002] confirm that deep metamorphic fluids migrate up on near vertical paths from a high strain zone in the root zone of the Southern Alps. Thus the location of the low-speed zone, and hence high pore pressure zone, directly above the region of highest reflection intensity is no coincidence (Plate 4). Permeability is enhanced by deformation and when the fluid pressure gets high enough fluid can advance along hydraulic fractures.

One of the consequences of enhanced fluid pressures in the crust is the effect on fault strength. The condition for sliding to occur on a pre-existing plane is [*King Hubbert and Rubey*, 1959]:

$$\tau_f = F\,(T_n - P_f) \qquad (7)$$

where τ_f is the shear traction at failure, F is the coefficient of friction, T_n is the normal traction on the fault and P_f is the fluid pressure. This well known relationship shows an increase in fluid pressure can cause a decrease in the differential stress required for shear failure on a fault, or for an array of faults that make up a fault zone [*Rice*, 1992].

6. LOWER CRUSTAL REFLECTIVITY AND DECOLLEMENT

An unmigrated, stack of CDP'98 shows two bands of reflections that converge westwards towards a central low point just to the west of Lake Pukaki (Plate 3a). Within the eastern part of the section we interpret the lower of two sub-parallel bands of strong reflectivity between 7 and 12 s twtt (20-35 km depth approximately) as a decollement surface between the mid- and lower crust for the following reasons. First, this reflectivity zone is prominent on our near vertical image but occurs at shallower depths than the Moho as determined from refraction and wide-angle reflection data [*Henrys et al.*, 2004] (Plate 3a). It is unclear why the Moho is not seen in the stack of vertical reflection data, but it could be because the Moho is gradational rather than abrupt. A second reason for the strong reflectivity to represent a decollement surface is that the reflectivity lies at the boundary between higher-velocity (>7 km/s) rocks and the quartz-schist type rock velocities of 6–6.2 km/s (Plate 3b). Thirdly, the high reflectivity zone can be tracked through to rocks exposed at the surface east of the Alpine Fault. These rocks are in essence identical to the full greywacke-schist crustal section seen in eastern South Island, albeit compressed into a thinner section. No mantle and only minor amounts of lower crustal rocks are brought up along the Alpine Fault.

7. MIGRATED SEISMIC REFLECTION IMAGE OF THE ALPINE FAULT ZONE

The steepest east-dipping reflectors located west of Lake Pukaki (Figure 5 and Plate 3a) are interpreted from shot gathers to be coming from a steeply dipping Alpine Fault and need to be correctly positioned using seismic migration methods. Industry-style and other migration methods give varying degrees of success [*Okaya et al.*, 2007]. The best migrated image using the western half of the CDP'98 data (Figure 2) suggests that the seismic data are imaging the Alpine Fault Zone in the depth range of 15–30 km (Plate 4a). At a depth of 15 km the fault zone is an inclined surface with steep dips (~60°), which then flattens and broadens into a sub-horizontal zone of strong reflectivity at a depth of about 30 km (Plate 4a).

One possible interpretation of the image is that the Alpine Fault is listric at depth and the fault flattens out near the surface. Such a flattening may be due to topographical smearing as the Alps are being progressively thrust westward. Migration of deep data will, however, produce some smearing and "smiles" [*Warner*, 1987] that may be present in our image. On the other-hand, confidence that the listric

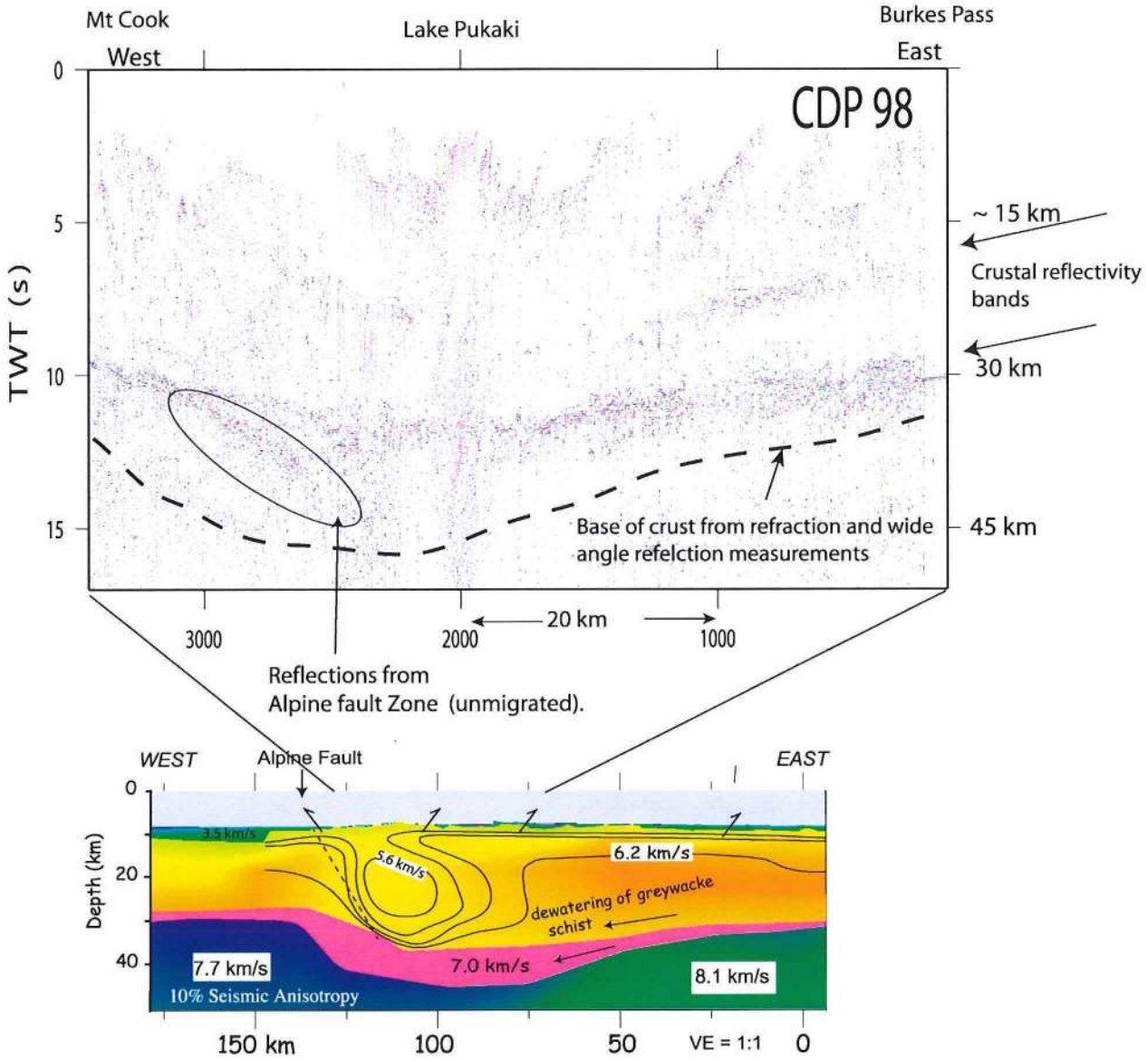

Plate 3. a. Stacked but unmigrated section of the CDP'98 survey from Burkes Pass to Mt Cook [*Okaya et al.,* 2007]. A total of 181 shots were detonated along the survey line. Sixty-five large (50 kg of explosives) shots were placed at 1 km intervals and buried 20 m deep. Smaller shots of 2.5 kg, buried 3 m deep, were located 250 m on either side of each large shot. Shot triggering was keyed on GPS time, to allow secondary piggy-back arrays to trigger without the need for direct radio communication. A total of 1000 geophone receiver group positions were used to record the shots, with a group spacing of 40 m. The number of recording channels for any one shot varied from a minimum of 400 to a maximum of 870. The maximum array aperture was nearly 35 km and the maximum shot receiver offset ~30 km. The raw seismic data for each shot were recorded to 30 s time, at a 2 ms sampling rate. Maximum fold is 12. Unmigrated Alpine Fault reflections are shown (in superposed ellipse region) cutting across the reflectivity from the lower crust. Depth scale on right is only approximate. b. Velocity model based on refraction data and wide-angle reflection inversion [*Scherwath et al.*, 2003]. Note that the strongest reflectivity in the stacked section (Plate 3a) corresponds to the lower-crust boundary that separates greywacke-schist rocks from mafic lower crust, possibly old oceanic crust. Variation in upper mantle wave speed has been interpreted as being due to ~10% mantle anisotropy

shape to the fault zone is real is gained by the strength of reflectivity within the westernmost sector.

If projected to the surface, the migrated reflections correspond to the surface trace of the Alpine Fault and the outcropping 1–2 km thick mylonite zone. It is unclear if the strong reflectivity in the depth range of 15–35 km also represents the highly foliated mylonite zone, but 2–5 times thicker than that observed at the surface. Geochemical evidence also shows the highest grade of schists thins by about 40% as they are exhumed [*Grapes and Watanabe*, 1992; *Grapes*, 1995].

A P-wave hitting the anisotropic [*Okaya et al.*, 1995] schist-mylonite rocks, perpendicular to the foliation, would produce a moderate reflection (Figure 6). Fluids being released by metamorphic reactions are, however, a more likely cause of the strong reflectivity given the close spatial relationship of the migrated reflectivity with the low velocity zone in the hanging wall of the Alpine Fault (Plate 4a), and the strength of Alpine Fault reflections (Figure 3 and Plate 2). Strong reflections can be produced by fluid being present in pockets of high concentration. Alternatively, fluids in just small concentrations (< 0.5 vol %) can weaken feldspathic rock and thus enhance and concentrate shear deformation [*Tullis and Tullis*, 1986]. A thick zone of shearing is also more likely to increase reflectivity by constructive interference [*Gough*, 1986].

Fluid enhanced shearing is our favoured interpretation of the strong reflectivity found in the lower crust beneath the Alps. The source of fluids is likely to be deep metamorphic fluids that geological [*Koons et al.*, 1998; *Vry et al.*, 2001] and geophysical [*Wannamaker et al.*, 2002] evidence suggest migrates up near vertical paths to the surface east of the Alpine Fault trace. The cause of the fluid release would be from both prograde metamorphism, linked to increased depth of burial [*Fyfe*, 1978], coupled with strain - induced metamorphism [*Koons et al.*, 1998]. The proposed pathway for the fluid is directly up through the low wave speed zone (Figure 13a, b). Thus this migrated seismic reflectivity data, combined with low-wave speed zone image, provides us with a new high-resolution image of both the source zone and pathway for fluids generated in the deep lower crust.

8. LOW SPEED, HIGH FLUID PRESSURE, STRONG REFLECTIVITY FAULTS AND SEISMICITY

As the rocks are detached from the lower crust and moved to the surface via the Alpine Fault Zone they are deformed. Mapping of exposed rocks within this zone shows it to be floored by ~1–2 km thick mylonites with shear fabrics subparallel to the dipping Alpine Fault Zone [*Wellman*, 1979; *Norris et al.*, 1990; *Norris and Cooper*, 2003; *Little*, 2004]. Above the mylonites, greywacke-schist rocks have been uplifted and sheared on near-vertical planes during the Cenozoic [*Little*, 2004] (Plate 4b). Pre-existing quartz veins within the greywacke-schist rock have been systematically offset across the shears in both brittle and ductile manners, probably during a steady (aseismic) creep process [*Little*, 2004; *Little et al.*, this volume; *Wightman and Little*, this volume].

Despite evidence for deep brittle behaviour, reconstructions of this deep region of the Alpine Fault Zone require the lithosphere here to be of low flexural rigidity since the lower crust has been deformed through a bend in transport direction with a tight radius of curvature (<10 km) (Plate 4b). This is also the region of anomalously low P-wave velocities, implying high fluid pressures and low strength, as discussed earlier. Thus an apparent contradiction exists in unusually deep reaching brittle behavior, within an otherwise weak crust.

An explanation for this apparent contradiction can be gained from an understanding of how high fluid pressure can effect the rheology of crustal rocks [*Sibson*, 1986]. Yield-stress envelopes are modified by an increase in pore pressure. For the case shown in Plate 4c, a move from hydrostatic to lithostatic fluid pressure leads to an increase in thickness of the brittle layer (embrittlement) from 8 to 22 km [*Meissner and Wever*, 1992]. At the same time there is a lowering of the maximum sustainable shear stress by nearly an order of magnitude. Thus a prediction of this fluid-related embrittlement process is that a deep region of brittle behaviour will result in more earthquakes of small magnitudes rather than fewer larger events distributed within a thinner brittle layer. This is a well known effect from injection of fluids in deep wells and impoundments of reservoirs [*Simpson*, 1986]. High strain rates may also contribute to the embrittlement process [*Little et al.*, this volume].

Recent results from active convergent plate boundaries show that fluid rich regions undergoing shear can radiate seismic energy in unusual ways. For example, non-volcanic, episodic tremor and slow-slip events have been noted in both Japan [*Obara*, 2002] and western Canada [*Rogers and Dragert*, 2003]. These appear to be linked to zones in the crust where fluids are plentiful and fluid pressure will be close to lithostatic. More specific associations are that metamorphically released fluid assists slip in shear zones at convergent margins [*Shelly et al.*, 2006] and that high pore pressure is the direct cause of silent slip events [*Kodaira et al.*, 2004].

Lateral Extent of Low Velocity Zone and Associated Weak Rheology

Seismicity for events M > 2 is restricted to the top 8 km beneath the central section of the Alpine Fault [*Leitner et al.*, 2001], roughly the depth at which the top of the low velocity

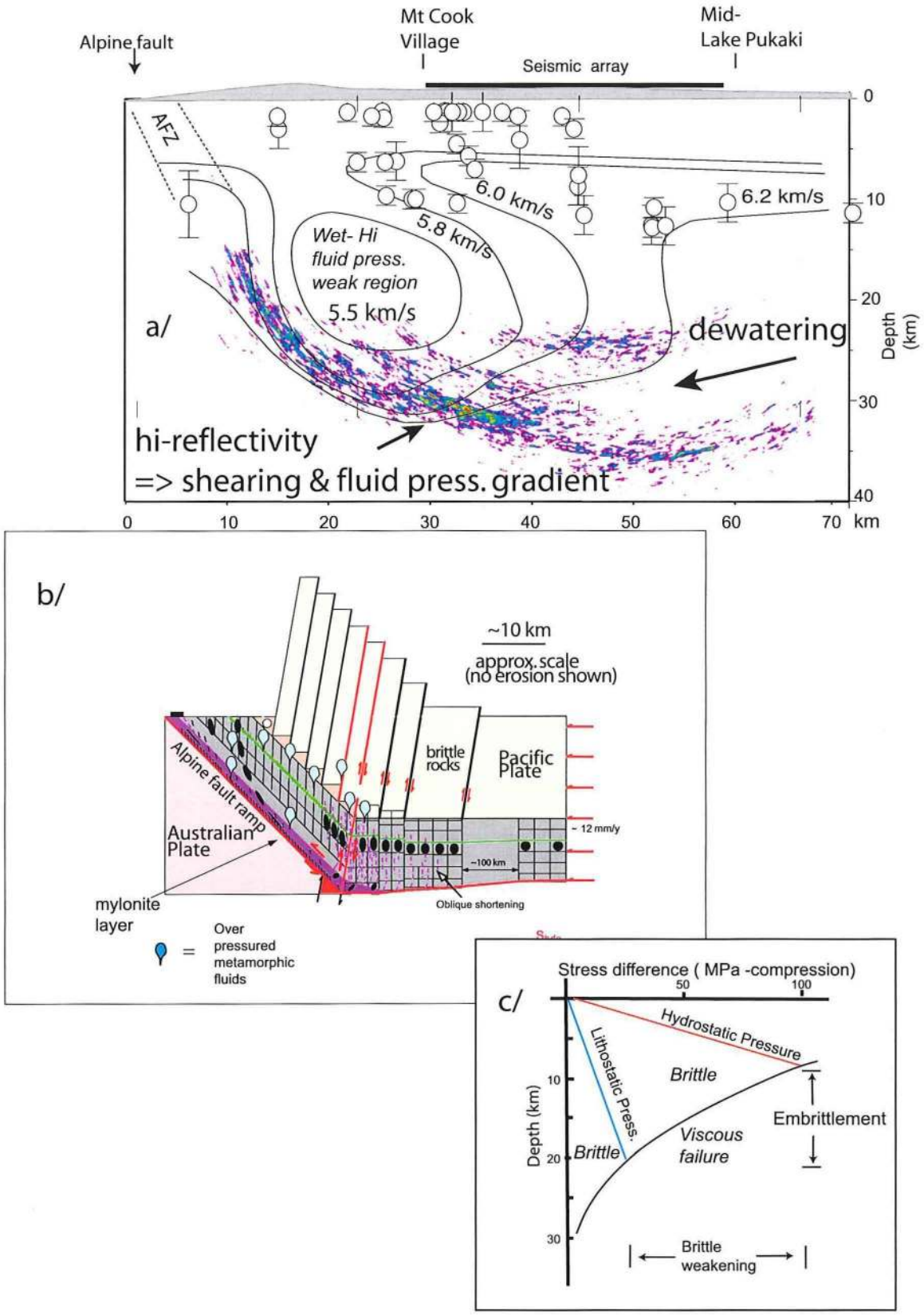
Alpine fault
Mt Cook Village
Mid-Lake Pukaki
Seismic array
AFZ
6.0 km/s
5.8 km/s
6.2 km/s
Wet- Hi fluid press. weak region
5.5 km/s
a/
dewatering
hi-reflectivity
=> shearing & fluid press. gradient
Depth (km)
0 10 20 30 40 50 60 70 km
b/
~10 km
approx. scale
(no erosion shown)
brittle rocks
Pacific Plate
Alpine fault ramp
Australian Plate
~ 12 mm/y
~100 km
Oblique shortening
mylonite layer
= Over pressured metamorphic fluids
c/
Stress difference (MPa -compression)
50
100
Hydrostatic Pressure
Lithostatic Press.
Brittle
Viscous failure
Embrittlement
Brittle
Depth (km)
10
20
30
Brittle weakening

zone is observed. One interpretation of the lack of seismicity below 8 km is that strain is accumulating in this part of the fault [*Sutherland et al.*, this volume]. An alternative interpretation of the scarce seismicity is that fluids have reduced the effective normal stress within the fault zone. Strain release is either as slow earthquakes and after slip, or as earthquakes below the M > 2.0 threshold for the most recent survey.

At the northern and southern ends of the central section of the Alpine Fault topography and rock uplift diminish [*Kamp and Tippett*, 1993]. Both crustal and mantle seismicity increase to the north and south of this central section [*Anderson and Webb*, 1994]. There is, therefore, an association of low seismic wave-speeds in the crust to both a lack of seismicity and high topography. A further distinctive aspect of the central section is a localised region of high exhumation rate in the region between Transects T1 and T2 [*Little et al.*, 2005]. The tightly clustered contours of mineral cooling age in this region resemble the data describing the "tectonic aneurysm" in the Himalayan syntaxes [*Zeitler et al.*, 2001].

Little et al. [2005] interpret the localised high exhumation zone as being due to changing geometry in the ramp up which rocks are exhumed. They propose a faulted backshear mode in the central section of the Alpine Fault (Plate 4b) compared to a broadly curved, unfaulted ramp further south. Why such a special mode of exhumation has developed in such a confined region remains unknown. We suggest the presence of excess fluids, high fluid pressure and reduced normal stress may also be factors that facilitate the development of the back shears.

9. MANTLE STRUCTURE AND DEFORMATION

During the shooting of the SIGHT program 160 seismographs were left running in continuous mode for about 7 days. Within this period three earthquakes from the western Pacific of $M_w \geq 5.0$ were recorded. As the azimuth of the path from the western Pacific to the west coast of South Island is nearly that of the seismic lines (Figure 1), arrivals from these events are treated like in–line shots with a large offset and a small incident angle (~25°) angle. These data were processed to produce plots of teleseismic P-wave delays along both transects [*Stern et al.*, 2000].

Two distinct trends can be seen in the teleseismic arrivals (Figure 10a): (a) a delay due to thickening of the crust beneath the Southern Alps (km 20–150) and (b) an advance of nearly a second between offsets of 40 to 100 km. Such a large advance in P-wave arrivals requires a region of high seismic wave-speed in the mantle. Tracing a ray back into the earth from the surface at km 100, where the maximum advance is observed, shows its path will be directly beneath the root of the Alps at a depth of 120 km (Figure 10a). This is consistent with relative high-speed mantle due to uniform thickening of a 100 km thick lithosphere that has been shortened by ~100 km [*Stern et al.*, 2000]. The shortened and relatively cold, denser and faster mantle lithosphere is displaced into the hotter, less dense and slower asthenosphere directly beneath the crustal root.

Six independent data sets were generated from the three earthquakes recorded on two transects. These data sets all suggest much the same structure - a roughly symmetric body, 2–17% faster than the surrounding mantle, which is located directly beneath the crustal root (Figure 14b). Our interpretation of the shape and position of this high-speed zone in the mantle is that it represents mantle lithosphere that has thickened and deformed in a ductile and continuous fashion. This is in contrast to intracontinental subduction that requires differential shear to be concentrated on a subduction thrust [e.g., *Koons*, 1990; *Beaumont et al.*, 1996]. Such a ductile and weak rheology may be linked to the 45 my of strike-slip shear causing both a pervasive heating [*Stern et al.*, 2000] and/or dynamic recrystallization in the mantle [*Scherwath et al.*, 2002].

A localized high-speed region in the mantle, in which P-wave speeds are 1–7% faster than in its surroundings, should also be denser than adjacent mantle and therefore contribute a gravity anomaly. Gravity analysis along T2 shows that the data are consistent with a mass anomaly of about 40 kg/m^3 in cross-section area of 120 × 80 km^2 [*Stern et al.*, 2000].

10. FLEXURAL RIGIDITY OF CENTRAL SOUTH ISLAND LITHOSPHERE

Much of the discussion on "strength" of faults has been based on noting that the directions of principal horizontal

Plate 4. (Opposite) a. Migrated version of the western portion of the stacked section shown in Plate 3 [*Okaya et al.*, 2007]. Superimposed on the stacked section are contours of the P-wave speed shown in (Figure 8a), and earthquake locations for events M >2 [*Leitner et al.*, 2001]. Interpreted regions of dewatering, shearing and high fluid pressure are shown. These data are based on the segment of profile that runs from Mt Cook Village to mid-way down Lake Pukaki (see dotted line on Figure 2). b. Cross-sectional interpretational model based on original concept of [*Wellman*, 1979] then modelled in detail by [*Little*, 2004]. Observations from the field suggest a combination of ductile and brittle behaviour to a depth of 20–25 km within the back shears. c. Yield stress envelop for compression under both hydrostatic and lithostatic fluid pressure [*Meissner and Wever*, 1992]. Note how a move from hydrostatic to lithostatic pressure creates an increase in the depth of brittle behaviour (embrittlement), and a drop in the maximum shear stress (brittle weakening).

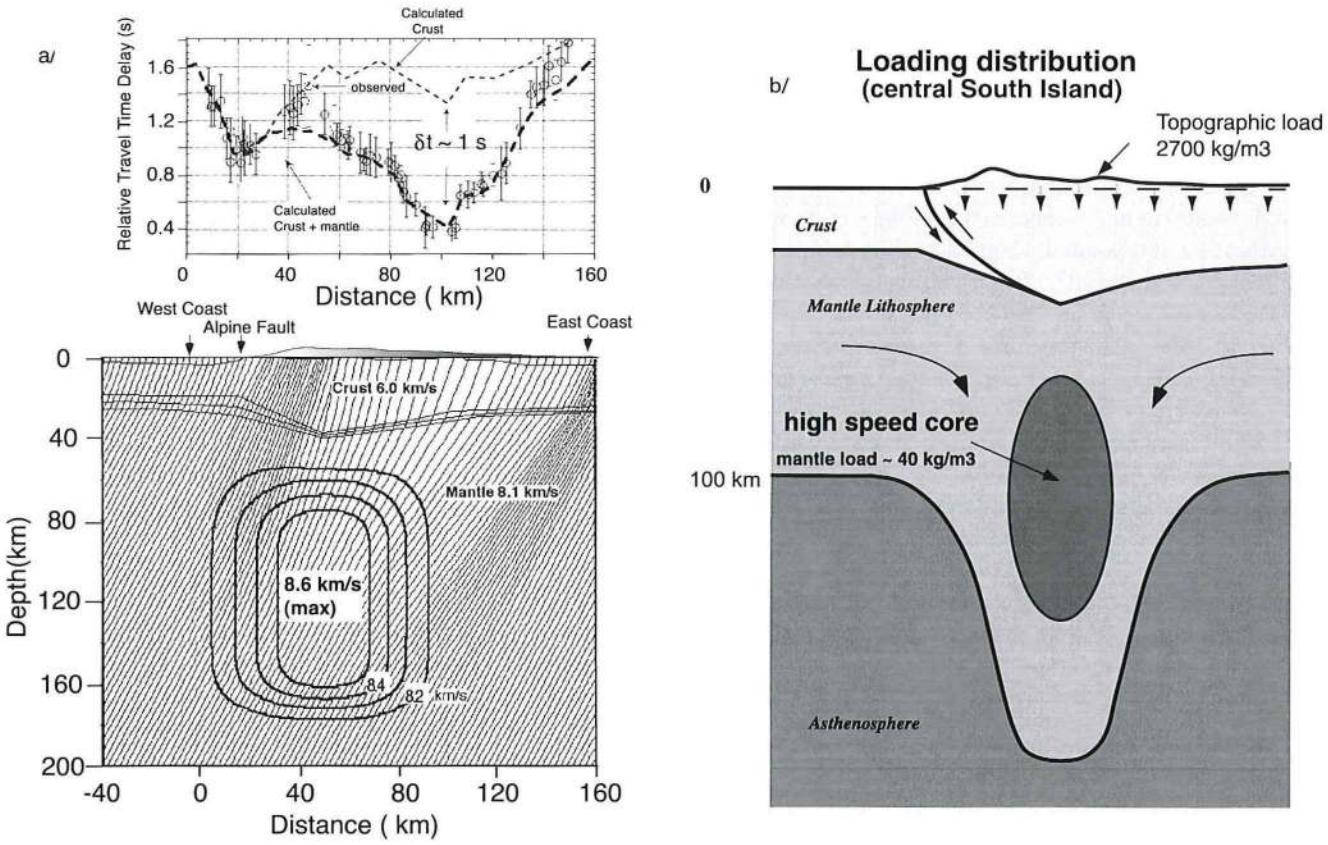

Figure 10. a. P-wave teleseismic delays from a Honshu earthquake recorded across transect 1. Delays (upper plot) are with respect to a standard earth model given by the IASP91 model [*Kennett and Engdahl*, 1991]. Note the positive delay (slowdown) associated with the crustal root then the major speed-up of (~δt = 1 s) that peaks at km 100. Delays have been corrected for elevation of stations above sea level. Distance is with respect to the west coast. Lightly dashed line represents fit for seismically determined crustal structure only. Heavy-dashed line represents fit of both crust and mantle structure. Bottom figure shows the ray-tracing of teleseismic waves from Honshu as they pass up through mantle and crust beneath central South Island. The velocity structure for the crust varies between 5.5 and 6.2 km/s, then 7.1 km/s for thin lower crustal layer. Mantle seismic wave speeds are 8.1 km/s except for symmetrical high-speed (max = 8.6 km/s) body that is required to sit directly beneath the crustal root. b. Cartoon showing tectonic interpretation of how high-speed zone in asthenosphere represents thickened, cold, and therefore fast and more dense, mantle lithosphere. Loading on the Moho is therefore in two parts: Surface topography and subsurface loading from the cold and therefore dense thickened mantle.

stress from fault plane solutions being at right angles to the fault zone [e.g., *Townend and Zoback*, 2001]. This only gives a relative sense of strength for the crust. Laboratory experiments have assisted in assessing the relative strength of various rock types, but these experiments are done at strain rates and temperatures much higher than what occurs in the earth [*Tullis and Tullis*, 1986]. We are also interested in how strong the plate boundary zone is, rather than just the Alpine Fault, and therefore seek a measure of both crust and mantle strength within and adjacent to the fault. Flexural rigidity provides such a measure of the gross strength of a sector of lithosphere [*Watts*, 2001]. To analyze flexure we need to measure the amplitude and wavelength of deformation induced by a known load. Critical to doing this is being able to identify a horizon that was once horizontal or planar, and is now deformed. Further, we must establish what the loading on the lithosphere is from loads within both the crust and mantle.

We assume the principal, vertical load acting on South Island is the "push" of topography and the "pull" of shortened mantle lithosphere (Figure 10b). A simple 2D gravity analysis shows that these two loads, although distributed in different

ways, are similar in magnitude [*Stern et al.*, 2000]. The Moho is used as a reference surface for this study of loading and flexure. Implicit in doing this is the assumption that the Moho was flat prior to collision and loading. Our justification for assuming a flat, pre-Pliocene Moho is based on the geological record of central South Island. Late Miocene shallow-marine sediments exist in all but the central alps, and shallow-water terrestrial sediments of early Pliocene age [*Gair*, 1967] are exposed over a wide region of central South Island, including the Mt. Cook region. Thus, prior to the main episode of loading at ~6 Ma muted topography and, therefore, a low relief Moho, are implied. A further assumption in using the Moho as a reference horizon is the lower and upper crust, and mantle lithosphere, all deform in unison.

Starting with a continuous elastic sheet, the effective elastic thickness (T_e), loading, and the restoring force from mantle buoyancy can be varied in an arbitrary manner via finite difference techniques (Figure 11) [*Bodine et al.*, 1981]. Principal loads on the elastic sheet are topography above sea level and the thickened mantle lithosphere. We also allow for a small load representing thrust sheet build up east of the Southern Alps into an assumed paleobathymetric depth of ~400 m. Justification for pre-Pliocene paleobathymetry east of the Southern Alps is based on geological evidence [*Stern*, 1995].

The effective elastic thickness (T_e) remains the variable to resolve from trial and error modeling [*Watts*, 2001]. The choice of a continuous, rather than a broken, or faulted, plate is more general and allows us to accommodate the concepts of a wide zone of deformation in the mantle and lower crust [*Molnar et al.*, 1999], while at the same time permitting us to approach the broken plate situation. Our best-fit variation of T_e is shown in Figure 11 and three fits to the deformed Moho are shown in Figure 12.

When both the topography and the shortened mantle are used as loads, and a constant T_e of 25 km, the resulting de-

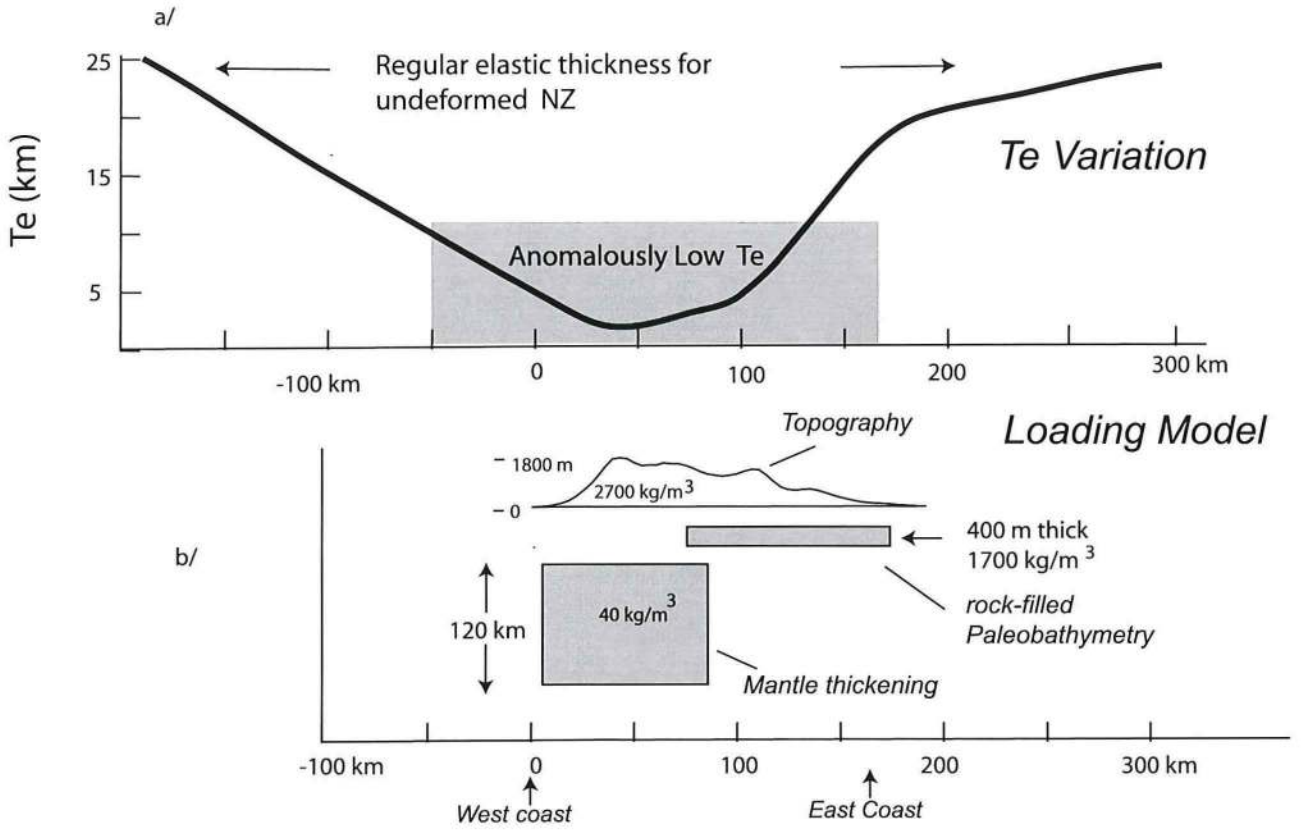

Figure 11. a. Plot showing the variation in T_e across central South Island that is required to explain the flexure of the Moho (see text). Note how T_e drops from regular value (T_e = 25 km) to a small value of T_e = 1 km beneath the central Alps. The region of anomalously small T_e (< 10 km) coincides with sub-aerial South Island. b. The two-dimensional distribution and magnitude of loads used in the flexure model. The rock filled paleobathymetry and smoothed topography is based on the gravity interpretation of *Stern* [1995] and the mantle load is based on the gravity interpretation model of *Stern et al.* [2000].

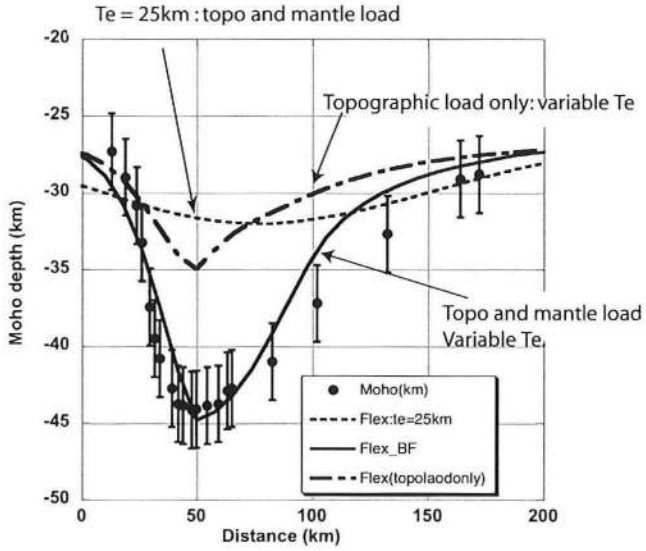

Figure 12. Flexure model for deformation of the Moho, central South Island based on the shape of the Moho (sold circles with error bars) from seismic measurements. Loading is based on model in Figure 11b. A continuous plate model is used and loading, elastic thickness (T_e) and restoring force are allowed to vary in an arbitrary fashion. Displacements (solid and dashed curves) are calculated using a finite-difference code [*Bodine et al.*, 1981] and compared to Moho picks (solid circles with ± 3 km errors bars). The Moho is assumed to have been flat and at a depth of 27 km prior to collision and loading. When both topographic and mantle loads are applied a T_e variation shown in Figure 11a is required to match (solid curve) the observed Moho displacement. Two curves are also shown that don't match the observations: dashed curve represents model where T_e is set to constant value of 25 km and loading is as shown in Figure 11b; dash-dot curve is for the topographic load using the T_e variation shown in Figure 15a.

flection does not match the Moho topography (Figure 12). Only when we allow T_e to drop to vanishingly small values in central South Island do we get a reasonable match in both wavelength and amplitude (Figure 12). Also shown is the predicted deflection of the Moho due to just topography loaded on a plate with the preferred T_e variation shown in Figure 11. Topography only provides sufficient loading to produce half the observed amplitude of the crustal root.

A value of T_e = 20–25 km is consistent with a well-constrained loading study on the western platform of New Zealand [*Holt and Stern*, 1991]. But values of T_e < 10 km that are required for most of subaerial central South Island are unusual [*Watts*, 2001], although many mountain ranges do show the same trend of a decrease of T_e towards their central regions [*Stewart and Watts*, 1997]. Such low values suggest that there is effectively no elastic strength in the mantle or crust, and strain and deformation is inferred to be accommodated by either ductile flow or upper crustal faulting. This observation is consistent with structural studies of veining and shearing discussed earlier [*Little et al.*, 2005]. What is new here is that there appears to be no contribution of flexural rigidity from the mantle. This is consistent with the mantle behaving in a ductile manner, and undergoing uniform thickening and distributed shear as advanced previously [*Molnar et al.*, 1999; *Stern et al.*, 2000; *Savage et al.*, this volume].

Ductile deformation and shortening of the mantle lithosphere is also consistent with the stark gap in subcrustal seismicity beneath central South Island [*Anderson and Webb*, 1994]. Some subcrustal earthquakes have, however, been reported [*Reyners*, 1987] beneath the central Southern Alps - the significance of which is still unclear.

11. DISCUSSION

The SIGHT program and its associated geological studies have demonstrated how central South Island is an optimal locality to image and study continental convergence. In particular, we have shown how a narrow continental island can be taken advantage of for advanced onshore-offshore seismic methods [*Okaya et al.*, 2002]. One of the central discoveries of SIGHT is the existence at depth of a broad Alpine Fault Zone where high fluid pressure and interconnected fluids in the crust are inferred. The depth and lateral extent (45 × 20 km) of the fault zone appears to be larger than for other continental transform faults [*Mooney and Ginzburg*,

1986; *Stern and McBride*, 1998]. Possible reasons for the successful image of the Alpine Fault Zone include its favorable inclined geometry that is optimal for seismic imaging, and the extreme exhumation rate east of the Alpine Fault [*Blythe*, 1998]. Strong exhumation would focus and enhance the dewatering process [*Koons et al.*, 1998] and would therefore accentuate the fluid-dependent geophysical anomalies we have described. Future experiments could be directed to exploring north and south of transects T1 and T2 to try and establish if the low–velocity, high-conductivity structures extend beyond the central Southern Alps. In addition, future experiments may benefit from more 3-component seismic instrumentation so we can target more directly the mechanical properties of the fault zone system.

Because of the discovery of a large zone of what is interpreted to be high fluid pressure in the Alpine Fault Zone, an analogy is drawn between it and the episodic slip and tremor documented in the subduction zones of Japan [*Obara*, 2002] and western Canada [*Rogers and Dragert*, 2003]. In these subduction zones the anomalous slip and tremor events are linked to water from dehydration and associated high-fluid pressures [*Julian*, 2002]. Even though the settings of the Alpine Fault Zone and these two subduction zones are different, the processes are similar. In both cases we are dealing with the seismological detection of dewatering. Because greywacke-schist rocks liberate water at lower temperatures and pressure than oceanic crust [*Fyfe*, 1978], the seismological image of the high fluid pressure region is shallower in central South Island than under Japan and western Canada. No episodic slip or tectonic tremor have been detected in central South Island. But as both Obara and Julian point out, with the present instrumentation in most other places, including New Zealand, they would not be detected. In this regard its is noteworthy that slow slip events have been detected on large continental faults that are distant from subduction zones, but where instrumentation is more advanced [*Kanamori*, 1989; *Kanamori and Hauksson*, 1992; *Linde et al.*, 1996]. Episodic tremor has also recently been reported from the San Andreas Fault [*Nadeau and Dolenc*, 2005].

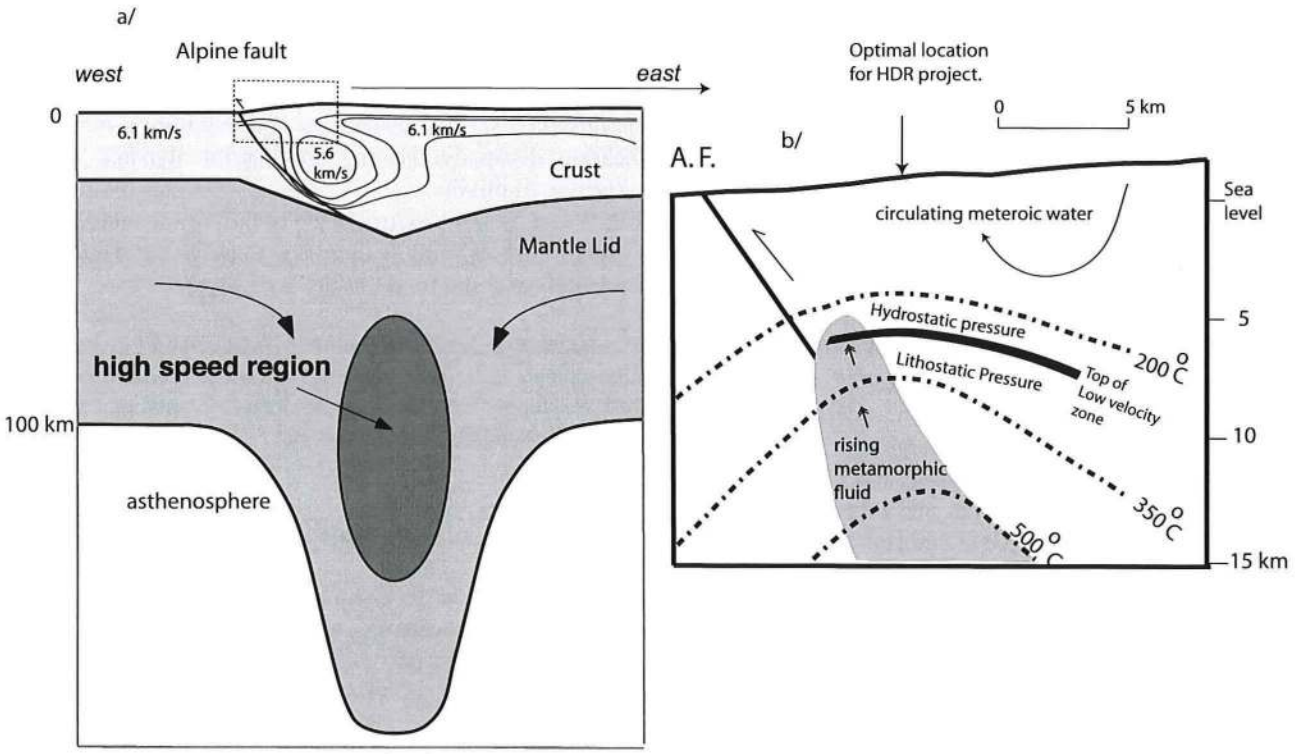

Figure 13. a. A summary of both crust-mantle structure showing crustal low velocity zone and inferred mantle thickening [*Stern et al.*, 2000]. Dashed box area shown in more detail in part b. b, A blow-up of crustal structure and fluid - phenomena in the top 10 km of crust east of the Alpine Fault Zone [*Wannamaker et al.*, 2001]. A suggested optimal position for a possible Hot-dry-rock power investigation is shown.

An important contribution of this study is an integration of data sets to give a larger picture of the strength of the plate boundary. What is seen, relative to regular parts of the continental lithosphere, is a region of vanishingly small flexural rigidity. Accordingly, most deformation in both the crust and mantle is inferred to be achieved by plastic flow and/or brittle faulting. Little or no long term elastic bending is evident. This does not, however, rule out short term (~300 yr) build up of elastic strain that could be released in large earthquakes [*Sutherland et al.,* this volume]. Nevertheless, the central Southern Alps low-velocity zone is a curious feature worthy of further study. It is clearly linked to the part of the Alpine Fault where anomalously fast exhumation is taking place, where topography is at a maximum, and geophysical and geological data show evidence of water at high pressure in the crust. Such regions are unusual for the middle to upper crust. It is possible, therefore, that this zone could act as a damper, that slows throughgoing ruptures by distributing strain more evenly in both space and time, and by anelastic processes.

There are potentially new insights from SIGHT to the study of resources. For example, future research might be directed at the thermal structure of the Alpine Fault Zone with a view to assess the zone for power generation by hot-water heat exchange methods. In Australia and Europe research is presently taking place into Hot-Dry Rock (HDR) exploration as a means of generating carbon-free electrical energy [*Barbier*, 2002]. In these projects ~5 km deep bore-holes are drilled into areas of high natural heatflow. The subsurface rock is hydro-fractured, water is pumped into these deep holes, allowed to become super-heated, then returned to the surface via other bore holes.

We suggest that the Alpine Fault Zone could be a favourable site for a HDR investigation for the following reasons. Firstly, HDR systems typically need rock temperatures of 200–250 °C, which according to most thermal and geophysical models (Figure 13) will be reached at depths of ~5 km [*Koons*, 1987; *Shi et al.*, 1996; *Wannamaker et al.*, 2002]. Secondly, there is a ready water supply from the west coast rivers, and that at a depth of 6 km our geophysical models predict that water will be tapped at lithostatic, or higher pressure. Thus, compared to some HDR projects elsewhere in the world, one centered here would need less drilling and no importing of water from other catchments.

12. CONCLUSIONS

We conclude our study of the Alpine Fault Zone with the following key points.

1. The Alpine Fault can be traced by seismic methods to a depth of about 35 km. The fault broadens with depth and appears to develop a listric shape.

2. Strong reflectivity zones are present in the root zone of the Alpine Fault that we infer to be shear-related. A calibrated attribute analysis shows that reflection coefficients are on the order of 0.25 and largely due to negative impedance contrasts. Anisotropy of the shear fabric, water filled voids and constructive interference could all contribute to this strong reflectivity.

3. We identify on the seismic reflection section a strong mid-crustal decollement surface along which crustal rocks are obducted to the surface and exhumed.

4. A zone of inferred high fluid pressures is defined within the Alpine Fault Zone by both low seismic P-wave velocity and high electrical conductivity. We interpret this zone as being due to water released by metamorphic reactions in the greywacke-schist as the crust is being thickened. Just as for dehydration processes in subduction zones, this zone may be critical in modulating the mode of strain release in the central section of the Alpine Fault.

5. A flexural loading study indicates that no long-term elastic strength is indicated for central South Island. T_e values recovery from near-zero values beneath the central Southern Alps to more normal values of ~20 km at the east and west coasts.

6. Weakening of the crust is linked to recent convergence, crustal thickening, prograde metamorphism and excess fluid pressure. In the mantle the lack of strength is consistent with the observed seismic anisotropy and therefore a history of shearing, dissipative heating, and possible dynamic recrystallisation of olivine.

7. We suggest the thermal state of the Alpine fault Zone is worthy of closer study with a view to assessing the top few kilometers as a site for a hot-dry-rock project.

Acknowledgements. We thank Peter Malin, Tim Little and one other anonymous reviewer for thorough and helpful reviews. This work was funded by NSF project EAR-9418530 and funding from the New Zealand Science Foundation.

REFERENCES

Anderson, H., and T. H. Webb (1994), New Zealand seismicity patterns revealed by the upgraded National Seismic Network, *N. Z. J. Geol. and Geophys., 37*, 477–493.

Barbier, E. (2002), Geothermal energy technology and current status: an overview, *Renewable and Sustainable Energy Reviews, 6*, 3–65.

Beaumont, C., P. J. J. Kamp, J. Hamilton, and P. Fullsack (1996), The continental collision zone, South Island, New Zealand; comparison of geodynamical models and observations., *J. Geophys. Res., 101*, 3333–3359.

Blythe, A. E. (1998), Active tectonics and Ultrahigh-pressure rocks, in When continents collide: Geodynamics and Geochemistry of

Ultrahigh-pressure Rocks, edited by B. R. Hacker, Liou. J. G., pp. 141–160, Kluwer Academic Publishers.

Bodine, J. H., M. S. Steckler, and A. B. Watts (1981), Observations of flexure and rheology of the oceanic lithosphere, *J. Geophys. Res., 86*, 3695–3707.

Davey, F. J., T. Henyey, S. Kleffmann, A. Melhuish, D. Okaya, T. A. Stern, and D. J. Woodward (1995), Crustal reflections from the Alpine Fault Zone, South Island, New Zealand., *N. Z. J. Geol. & Geophys., 38*, 601–604.

Davey, F. D., T. Henyey, W. S. Holbrook, D. Okaya, T. A. Stern, A. Melhuish, S. Henrys, D. Eberhart-Phillips, T. McEvilly, R. Urhammer, H. Anderson, F. Wu, G. Jiracek, P. Wannamaker, G. Caldwell, and N. Christensen, (1997), Preliminary results from a geophysical study across a modern, continent-continent collisional plate boundary - the Southern Alps , New Zealand., *Tectonophysics, 288*, 221–235.

Dobrin, M. B. (1976), Introduction to Geophysical Prospecting, 630 pp., McGraw-Hill, New York.

Fyfe, W. S., N. J. Price, and A. B. Thompson (1978), Fluids in the Earth's Crust, 383 pp., Elsevier, New York.

Gair, H. S. (1967), Sheet 20 - Mt Cook. Geological map of New Zealand, 1:250,000, Department of Scientific and Industrial Research, Wellington.

Garrick, R., and T. Hatherton (1973), Seismic velocity studies in the Southern Alps, New Zealand, *N. Z. J. Geol & Geophys, 16*, 973–995.

Gough, D. I. (1986), Seismic reflectors, conductivity, water and stress in the continental crust, *Nature, 323*, 143–147.

Grapes, R. H. (1995), Uplift and exhumation of Alpine Schist, Southern Alps, New Zealand., *N. Z. J. Geol. & Geophys., 38*, 525–534.

Grapes, R. H., and T. Watanabe (1992), Metamorphism and uplift of the Alpine schist in the Franz Josef-Fox Glacier area, Southern Alps, New Zealand, *J. Metamorph. Pet., 10*, 171–180.

Henrys, S. H., D. J. Woodward, D. Okaya, and J. Yu (2004), Mapping the Moho beneath the Southern Alps continent-continent collision, New Zealand, using wide-angle reflections, *Geophys. Res. Lett., 31*, doi:10.1029/2004GLO20561.

Hickman, S., M. D. Zoback, and W. Ellsworth (2004), Introduction to special sections: Preparing for the San Andreas Fault Observatory at Depth, *Geophys. Res. Lett., 31*, L12S01, doi:10.1029/2004GL020688.

Hole, J. A. (1996), Seismic reflections from the near vertical San Andreas Fault., *Geophys. Res. Lett., 23*, 237–240.

Hole, J. A., R. D. Catchings, K. C. St Clair, M. J. Rymer, D. Okaya, and B. J. Carney (2001), Steep-dip seismic imaging of the shallow San Andreas Fault near Parkfield, *Science, 294*, 1513–1515.

Holt, W. E., and T. A. Stern (1991), Sediment loading on the Western Platform of the New Zealand continent: Implications for the strength of a continental margin, *Earth Planet. Sci. Lett., 107*, 523–538.

Jones, T. D., and A. Nur (1984), The nature of seismic reflections from deep crustal fault zones, *J. Geophys. Res., 89*, 3153–3171.

Julian, B. (2002), Seismological detection of slab metamorphism, *Science, 296*, 1625–1626.

Kamp, P. J., and J. M. Tippett (1993), Dynamics of Pacific Plate crust in the South Island (New Zealand) zone of oblique continent-continent convergence, *J. Geophys. Res., 98*, 16,105–116,118.

Kanamori, H. (1989), A slow seismic event recorded in Pasadena, *Geophys. Res. Lett., 16*, 1411–1414.

Kanamori, H., and E. Hauksson (1992), A slow earthquake in the Santa Maria Basin, California, *Bull. Seis. Soc. Am., 82*, 2087–2096.

Kennett, B. L. N., and E. R. Engdahl (1991), Travel times for global earthquake location and phase identification, *Geophys. J. Int., 105*, 429–465.

King Hubbert, M., and W. W. Rubey (1959), Role of Fluid pressure in mechanics of overthrust faulting, *Bull. Geol. Soc. Am., 70*, 115–166.

Kleffmann, S. (1999), Crustal structure studies of a transpressional plate boundary - the central South Island of New Zealand, PhD thesis, 233 pp, Victoria University of Wellington, Wellington.

Kleffmann, S., F. Davey, A. Melhuish, D. Okaya, and T. Stern (1998), Crustal structure in the central South Island from the Lake Pukaki seismic experiment., *N. Z. J. Geol. Geophys., 41*, 39–49.

Kodaira, S., T. Iidaka, A. Kato, J. O. Park, T. Iwasaki, and Y. Kaneda (2004), High Pore Fluid Pressure May Cause Silent Slip in the Nankai Trough, *Science, 304*, 1295–1298.

Koons, P. O. (1987), Some thermal and mechanical consequences of rapid uplift: an example from the Southern Alps, New Zealand, *Earth Planet. Sci. Lett., 86*, 307–319.

Koons, P. O. (1990), Two-sided orogen; collision and erosion from the sandbox to the Southern Alps, New Zealand, *Geology, 18*, 679–682.

Koons, P. O., D. Craw, S. C. Cox, P. Upton, A. S. Templeton, and C. P. Chamberlain (1998), Fluid flow during active oblique convergence: A Southern Alps model from mechanical and geochemical observations, *Geology, 26*, 159–162.

Leitner, B., D. Eberhart-Phillips, H. Anderson, and J. Nabeleck (2001), A focussed look at the Alpine fault, New Zealand: seismicity, focal mechanisms, and stress observations, *J. Geophys. Res., 106*, 2193–2220.

Linde, A. T., M. T. Gladwin, M. J. S. Johnston, R. L. Gwyther, and R. G. Bilham (1996), A slow earthquake sequence on the San Andreas fault, *Nature, 383*, 65–68.

Little, T. A. (2004), Transpressive ductile flow and oblique ramping of lower crust in a two-sided orogen: Insight from quartz grain-shaped fabrics near the Alpine Fault, New Zealand, *Tectonics*, doi:10.1029/2002TC001456.

Little, T. A., S. Cox, J. K. Vry, and G. Batt (2005), Variations in exhumation level and uplift rate along the oblique-slip Alpine fault, central Southern Alps, *GSA Bull., 117*, 707–723.

Little et al. (this volume), Transpression models and ductile deformation of the lower crust of the Pacific Plate in the central Southern Alps, a perspective from structural geology

Little, T., R. Wightman, R. J. Holcombe, and M. Hill (this volume), Transpression models and ductile deformation of the lower crust of the Pacific Plate in the central Southern Alps, a perspective from structural geology.

Meissner, R., and T. Wever (1992), The possible role of fluids for the structuring of the continental crust, *Earth Sci. Rev., 32*, 19–32.

Molnar, P., H. Anderson, E. Audoine, D. Eberhart-Philips, K. Gledhill, E. Klosko, T. McEvilly, D. Okaya, M. Savage, T. Stern,

and F. Wu (1999), Continuous deformation versus faulting through the continental lithosphere of New Zealand, *Science, 286*, 516–619.

Mooney, W. D., and A. Ginzburg (1986), Seismic measurements of the internal properties of fault zones, *Pure. Appl. Geophys., 124*, 141–157.

Nadeau, R. M., and D. Dolenc (2005), Nonvolcanic tremors deep beneath the San Andreas Fault, *Science, 307*, 389.

Norris, R. J., and A. F. Cooper (2003), Very high strains recorded in mylonites along the Alpine Fault, New Zealand: implications for the deep structure of plate boundary faults, *J. of Struct. Geol., 25*.

Norris, R. J., P. O. Koons, and A. F. Cooper (1990), The obliquely convergent plate boundary in the South Island of New Zealand; implications for ancient collision zones, *J. Struct. Geology, 12*, 715–725.

Obara, K. (2002), Nonvolcanic deep tremor associated with subduction in southwestern Japan, *Science, 296*, 1679–1681.

Okaya, D., N. Christensen, D. Stanley, and T. Stern (1995), Crustal anisotropy in the vicinity of the Alpine Fault Zone , South Island New Zealand., *N. Z. J. Geol. & Geophys.*, 38, 579–584.

Okaya, D., S. Henrys, and T. Stern (2002), Double-sided onshore-offshore seismic imaging of a Plate Boundary: Super-gathers across South Island of New Zealand, *Tectonophysics, 355*, 247–263.

Okaya, D., T. A. Stern, and S. H. Henrys (2007), Seismic image of continental collision at a transform plate boundary, New Zealand, *Science, submitted*.

Pulford, A., M. K. Savage, and T. A. Stern (2003), Absent anisotropy: the paradox of the Southern Alps orogen, *Geophys. Res. Lett.*, doi:10.1029/2003GL017758.

Reyners, M. (1987), Subcrustal earthquakes in the central South Island, New Zealand, and the root of the Southern Alps, *Geology, 15*, 1168–1171.

Rice, J. R. (1992), Fault stress states, pore pressure distributions, and the weakness of the San Andreas fault., in Fault mechanics and the transport properties of rocks, edited by B. Evans and T. F. Wong, pp. 475–504, Academic Press, New York.

Rogers, G., and H. Dragert (2003), Episodic tremor and slip: the chatter of slow earthquakes, *Science, 300*, 1942–1944.

Savage et al. (this volume).

Scherwath, M., T. Stern, A. Melhusih, and P. Molnar (2002), Pn anisotropy and distributed upper mantle deformation associated with a continental transform fault, *Geophys. Res. Lett.*, doi:10.1029/2001GL014179.

Scherwath, M., T. A. Stern, F. J. Davey, D. Okaya, W. S. Holbrooke, R. Davies, and S. Kleffmann (2003), Lithospheric structure across oblique continental collision in New Zealand from wide-angle P-wave modeling, *J. Geophys. Res.*, doi:10.1029/2002JB002286.

Scholz, C. (2000), Evidence for a strong San Andreas fault., *Geology, 28*, 163-166.

Shelly, D. R., G. C. Beroza, S. Ide, and S. Nakamula (2006), Low-frequency earthquakes in Shikoku, Japan, and their relationship to episodic tremor and slip, *Nature, 442*, 188–191.

Sheriff, R. E., and L. P. Geldart (1995), Exploration Seismology, 2nd ed., 592 pp., Cambridge University Press.

Shi, Y., R. Allis, and F. Davey (1996), Thermal modelling of the Southern Alps, *Pure. Appl. Geophys., 146*, 469–501.

Sibson, R. H. (1986), Earthquakes and rock deformation on a crustal fault, *Ann. Rev. Earth Planet. Sci., 14*, 149–176.

Simpson, D. W. (1986), Triggered earthquakes, *Ann Rev. Earth and Planet Sci., 14*, 21–42.

Smith, E. G., C., T. Stern, and B. O'Brien (1995), A seismic velocity profile across the central South Island, New Zealand, from explosion data, *N. Z. J. Geol. Geophys.*, 38, 565–570.

Stern, T., S. Kleffmann, D. Okaya, M. Scherwath, and S. Bannister (2001), Low seismic wave-speeds and enhanced fluid pressure beneath the Southern Alps, New Zealand, *Geology, 29*, 679–682.

Stern, T. A. (1995), Gravity anomalies and crustal loading at and adjacent to the Alpine Fault, New Zealand, *N. Z. J. Geol. Geophys., 38*, 593–600.

Stern, T. A., and J. H. McBride (1998), Seismic exploration of strike-slip zones, Special issue: Deep Seismic Profiling of the Continents: General Results and New Methods, *Tectonophysics, 286*, 63–78.

Stern, T. A., P. Molnar, D. Okaya, and D. Eberhart-Phillips (2000), Teleseismic P-wave delays and modes of shortening the mantle beneath the South Island, New Zealand, *J. Geophys. Res., 105*, 21,615–621,631.

Stewart, J., and A. B. Watts (1997), Gravity anomalies and spatial variations of flexural rigidity at mountain ranges, *J. Geophys. Res., 102*, 5327–5352.

Sutherland, R., D. Eberhart-Phillips, R. A. Harris, T. Stern, J. Beavan, S. Ellis, S. Henrys, S. Cox, R. J. Norris, K. R. Berryman, J. Townend, S. Bannister, J. Pettinga, B. Leitner, L. Wallace, T. A. Little, A. F. Cooper, M. Yetton, and M. Stirling (this volume), Do great earthquakes occur on the Alpine fault in central South Island, New Zealand?

Townend, J., and Z. Zoback (2001), Implications of earthquake focal mechanisms for the frictional strength of the San Andreas fault system, Special Publication of the geological Society of London, in press.

Tullis, T. E., and J. Tullis (1986), Experimental rock deformation techniques., in Mineral and Rock Deformation: Laboratory Studies, edited by B. E. Hobbs, Heard, H. C., American Geophysical Union, Washington.

van Avendonk, H., W. S. Holbrook, D. Okaya, J. Austin, F. Davey, and T. Stern (2004), Continental crust under compression: A seismic reflection study of South Island Geophysical Transect 1, South Island, New Zealand, *J. Geophys. Res., 109*, doi:10.1029/2003JB002790.

Vry, J. K., A. C. Storkey, and C. Harris (2001), Role of fluids in the metamorphism of the Alpine Fault Zone, New Zealand, *J. Metamorphic Geol., 19*, 21–31.

Wannamaker, P. E., G. R. Jiracek, J. A. Stodt, T. G. Caldwell, V. M. Gonzalez, J. D. McKnight, and A. D. Porter (2002), Fluid generation and pathways beneath an active compressional orogen, the New ZealandSouthern Alps, inferred from magnetotelluric data, *J. Geophys. Res., 107*, 2117, doi2110.1029/2001JB000186.

Warner, M. (1987), Migration — why doesn't it work for deep continental data?, *Geophys. J. R. astron. Soc., 89*, 21–26.

Warner, M. (1990), Absolute reflection coefficients from deep seismic reflections, *Tectonophysics, 173*, 15–23.

Warner, M. (2004), Free water and seismic reflectivity in the lower continental crust, *J. of Geophysics and Engineering, 1*, 88–101.

Watts, A. B. (2001), Isostasy and flexure of the lithosphere, 458 pp., Cambridge University Press.

Wellman, H. W. (1979), An uplift map for the South Island of New Zealand, *Bull. Roy. Soc. N. Z., 18*, 13–20.

Wightman, R. H., and T. A. Little (this volume), Deformation of the Pacific Plate above the Alpine Fault ramp and its relationship to expulsion of metamorphic fluids: an array of backshears.

Zeitler, P. K., A. S. Meltzer, P. O. Koons, D. Craw, B. Hallet, C. P. Chamberlin, W. S. F. Kidd, S. K. Park, L. Seeber, M. Bishop, and J. Shroder (2001), Erosion, himalayan geodynamics, and the geomorphology of metamorphism, *GSA Today, 11*, 4–9.

Zoback, M. (2000), Strength of the San Andreas, *Nature, 405*, 31.

Fred Davey and Stuart Henrys, Institute of Geological and Nuclear Sciences, Lower Hutt, New Zealand.

Stefan Kleffmann, New Zealand Oil and Gas, Wellington, New Zealand.

David Okaya, Department of Earth Sciences, University of Southern California, Los Angeles, CA, USA.

Martin Scherwath, GEOMAR, Kiel, Germany.

Tim Stern, School of Earth Sciences, Victoria University of Wellington, Wellington, New Zealand.